

DESIGN OF A MAGNETIC LENS  
MONOENERGETIC ELECTRON SOURCE

by

RICHARD A. WEINER

B.S. in N.E., Kansas State University, 1987

B.S. in E.E., Kansas State University, 1989

---

MASTER'S THESIS

submitted in partial fulfillment of the  
requirements for the degree

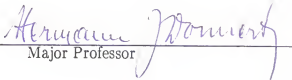
MASTER OF SCIENCE

Department of Nuclear Engineering

Kansas State University

Manhattan, Kansas

1989

  
Major Professor

LD  
2668  
.T4  
NE  
1989  
W45  
C.2

# TABLE OF CONTENTS

A11208 317274

	PAGE
I. INTRODUCTION . . . . .	1
II. THEORY OF OPERATION AND TERMINOLOGY . . . . .	4
III. VACUUM CHAMBER AND COIL DESIGN . . . . .	7
3.1. SELECTION OF THE MAGNETIC FIELD SHAPE . . . . .	8
3.2. SELECTION OF THE CENTRAL-RAY INITIAL EMISSION ANGLE . . . . .	11
3.3. DETERMINATION OF VACUUM CHAMBER DIMENSIONS . . . . .	12
3.4. DESIGN OF THE MAGNET COIL . . . . .	15
IV. THEORETICAL OPERATIONAL ANALYSIS . . . . .	17
4.1. DERIVATION OF THE EQUATIONS OF MOTION . . . . .	18
4.2. DERIVATION OF THE MAGNETIC FLUX- DENSITY VECTOR . . . . .	20
4.3. SOLUTION OF THE EQUATIONS OF MOTION . . . . .	31
4.3.1. DETERMINATION OF THE RANGE OF ALLOWED INITIAL EMISSION ANGLES. . . . .	33
4.3.2. DETERMINATION OF THE SOURCE AND FOCAL POINT POSITIONS. . . . .	35
4.3.3. DETERMINATION OF THE SPECTROMETER OPERATING EQUATION. . . . .	37
4.3.4. DETERMINATION OF THE RING FOCUS POSITION . . . . .	40
4.3.5. DETERMINATION OF THE COLLIMATION ANGLE. . . . .	10
4.3.6. ADDITIONAL INFORMATION GENERATED BY PATH-RK4 . . . . .	13
4.4. DETERMINATION OF TRANSMISSION AND RESOLUTION CHARACTERISTICS . . . . .	51
4.4.1. RESOLUTION VARIATION WITH BEAM ENERGY . . . . .	59
4.4.2. TECHNIQUE TO IMPROVE THE BASE WIDTH RESOLUTION . . . . .	59
4.4.3. OBSERVATIONS AND CONCLUSIONS REGARDING RESOLUTION . . . . .	61
V. POWER SUPPLY STABILITY REQUIREMENTS . . . . .	66
VI. CONCLUSION . . . . .	69
VII. REFERENCES . . . . .	70

VIII. APPENDICES . . . . .	71
A. COMPUTER PROGRAMS	
B. DERIVATION OF THE APPROXIMATE AVERAGE AXIAL MAGNETIC FIELD COMPONENT INSIDE A SOLENOID OF FINITE LENGTH	

## LIST OF FIGURES

FIGURE	CAPTION	PAGE
1.1	Scale model of the Kansas State University magnetic lens monoenergetic electron source (KSU-MLMES#1). The ray traces depicted correspond to beta-particles emitted from the center face of a disk source with initial emission angles $\alpha \pm \alpha$ . . . . .	3
2.1	Typical beta spectrum from a $^{90}\text{Sr}/^{90}\text{Y}$ source [10]. . . . .	5
3.1	Resolution characteristics of several typical magnetic lens spectrometer field shapes as a function of the central-ray initial emission angle [11-13]. Field shape 24 was selected for the design of KSU-MLMES#1. . . . .	9
3.2	End-view of the vacuum chamber with the end-view of the central-ray trajectory inscribed. Note that the vacuum chamber diameter must be at least twice the maximum diameter of the end-view of the central-ray trajectory. . . . .	14
4.1	Geometry of the coil utilized in evaluating the magnetic flux-density vector. The differential magnetic field strength ( $\vec{\Delta}\mathbf{B}$ ) at the point (p,h) generated by a differential current element ( $\vec{\Delta}dV$ ) is depicted . . . . .	21
4.2	Shape of the axial component of the magnetic field along the solenoid at several radial positions. Division of $B_z$ by the electric current (I) yields relative field shape information that is only a function of the physical geometry of the coil. . . . .	27
4.3	Shape of the radial component of the magnetic field along the solenoid at several radial positions. Division of $B_r$ by the electric current (I) yields relative field shape information that is only a function of the physical geometry of the coil. . . . .	28
4.4	Transverse shape of the axial component of the magnetic field at several axial positions . . . . .	29
4.5	Transverse shape of the radial component of the magnetic field at several axial positions. . . . .	30

FIGURE	CAPTION	PAGE
4.6	Ray traces for a variety of source positions that were examined to determine appropriate source position. Source positions: 1) maximum at which central-ray symmetric focusing occurs, and 2) selected source position . . .	36
4.7	Transverse shape of the axial component of the magnetic field at several axial positions. . . . .	38
4.8	The radial component of the helical trajectory versus axial position of particles emitted from a point source at angles $\alpha \pm \Delta\alpha$ (corresponding to 1% transmission). The figure clearly indicates the annular focusing that is typical of magnetic lens spectrometer systems. . . . .	41
4.9	Magnified view of the point source ring focus position . . . . .	42
4.10	Central-ray trajectory versus axial position in rectangular and cylindrical coordinates. Note that the r vs. z trace appears to be symmetric about the plane $z=0$ ; however, the individual rectangular making up r (i.e. x and y are not symmetric. . . . .	44
4.11	Shape of the radial component of the magnetic field experienced by a beta-particle as it travels along the central-ray trajectory. $B_r$ is divided by the electric current (I) to yield relative field shape information that is independent of particle energy. . . . .	45
4.12	Shape of the axial component of the magnetic field experienced by a beta-particle as it travels along the central-ray trajectory. $B_z$ is divided by the electric current (I) to yield relative field shape information that is independent of particle energy . . . . .	46
4.13	Rectangular velocity components of a 1 MeV beta-particle traveling along the central-ray trajectory. Note that the velocity components at the focal point are not the same as at the source point. . . . .	47
4.14	Two dimensional (x versus y) end-view of the central-ray trajectory. Note that the velocity components at the focal point are not the same as at the source point . . . . .	48

FIGURE	CAPTION	PAGE
4.15	r versus z ray traces for particles of selected energy emitted at extremum angles $\alpha_{1a}$ , $\alpha_2$ , $\alpha_3$ , $\alpha_4$ and from the center of a disk source at $\alpha$ and $\alpha \pm \Delta\alpha$ .	52
4.16	The solid lines depict ray traces of particles of selected energy (1 MeV) emitted at the extremum angles about the periphery of a disk source of diameter = 1 cm. The dotted lines depict traces made by the maximum and minimum energy particles that contribute to the beam emitted from the extremum angles. The cross hatched region depicts portions of the beam that do not contain any particles of selected energy. Collimator sets 1 and 2 are configured for T = 1%.	54
4.17	Theoretical base-width resolution as a function of disk source diameter for 0.5% and 1% transmissions. Data are for the system configured with collimators 2a and 2b positioned to accept all particles of selected energy reaching collimator set 2.	58
4.18	Theoretical variation in the base-width resolution with source diameter and selected beam energy. Data are for a system configured for 1% transmission and with collimators 2a and 2b positioned to accept all particles of selected energy reaching collimator set 2.	60
4.19	Monoenergetic electron peaks generated by the National Bureau of Standards 4 MeV Van de Graaff accelerator. Degradation in air of nominal 200 keV to 2.5 MeV electrons in different thicknesses of intervening air layers [16].	63
4.20	Monoenergetic electron peak generated by the Lawrence National Laboratory magnetic lens monoenergetic electron source [9].	64
5.1	Selected beam energy dispersion as a function of electric current.	67

## LIST OF TABLES

TABLE	CAPTION	PAGE
4.1	The kinetic energy of particles that will be focused for a specified electric current. The data was generated by an iterative application of the program PATH-RK4. . . . .	37
4.2a	The extremum angles, maximum and minimum particle energies contributing to the beam, and the theoretical base-width resolution for a point source and sources of diameter 0.1, 0.6, and 1.0 cm. All data are for a selected beam energy of 1 MeV and 1% transmission. . . . .	56
4.2b	The extremum angles, maximum and minimum particle energies contributing to the beam, and the theoretical base-width resolution for a point source and sources of diameter 0.1, 0.6, and 1.0 cm. All data are for a selected beam energy of 1 MeV and 0.5% transmission. . . . .	57

## I. INTRODUCTION

The Nuclear Engineering department at Kansas State University is involved in researching beta particle dosimetry and instrumentation. To facilitate the calibration of beta scintillator and germanium crystal detection systems, as well as for the purpose of materials energy response characterization, a source of monoenergetic electrons is useful. This thesis describes the design of a high resolution monoenergetic electron source based upon the concept of a solenoidal magnetic lens spectrometer.

Magnetic lens spectrometer (MLS) systems were conceived by Kapitza [1] in 1923 and first constructed by Tricker [2] in 1924. From the 1940's, Witcher [3], Klemperer [4], Deutsch, Elliot and Evans [5], DuMond [6], Persico [7], and Schmidt [8] amongst others have pursued the development of MLS systems. Initially MLS systems were used for the purpose of characterizing the emissions from beta and conversion electron sources, and photoelectrons emitted by gamma rays incident upon target materials. In 1983, Graham and Elliot [9] converted a MLS system at Lawrence National Laboratory into a cheap source of monoenergetic electrons. Comparisons will be drawn between the magnetic lens monoenergetic electron source at Lawrence National Laboratory which will be referred to as (LNL-MLMES) and the system design arrived at in this thesis.

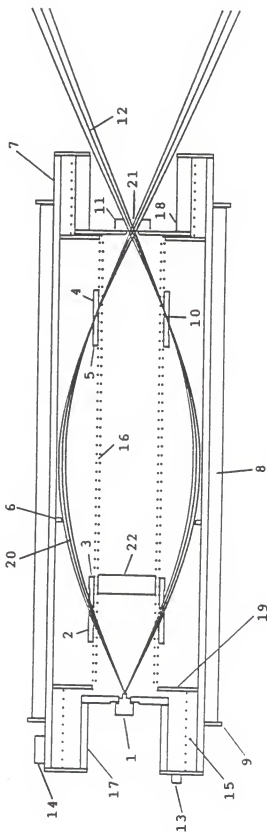
A design of a MLMES was arrived at with the following specifications:

- 1) continuously selectable monoenergetic electron beam with energy ranging from 100 keV to 2.84 MeV
- 2) central ray initial emission angle of  $25^{\circ}$  and allowed emission angle range  $23.644^{\circ}$  to  $26.356^{\circ}$  for 1.0% transmission



- 3) transmission of 1.0% (transmission is defined as the fraction of the particles of selected energy emitted from a point source that are accepted by the first collimator)
- 4) central-ray helical particle trajectory with pitch or "focal length" of 0.762 m
- 5) vacuum chamber (1.016 m long by 0.254 m i.d.)
- 6) magnet coil (1196 turns, #6 A.W.G. aluminum wire) resistance= $2.38 \Omega$  at  $25^{\circ}\text{C}$ , inductance= $0.13 \text{ H}$
- 7) vacuum requirement of 0.1 torr [9]

A schematic of the KSU MLMES is provided in fig. (1.1).



LIST OF MLMES STRUCTURAL COMPONENTS AND TRAJECTORY TERMINOLOGY

- |                          |  |
|--------------------------|--|
| 1) SOURCE                | 14) ELECTRICAL TERMINATION STRIP                       |
| 2) COLLIMATOR 1A         | 15) COLLIMATOR STRUCTURE POSITIONING SPACER            |
| 3) COLLIMATOR 1B         | 16) COLLIMATOR POSITIONING AND SUPPORT TUBE            |
| 4) COLLIMATOR 2A         | 17) SOURCE HOLDER AND SUPPORT TUBE                     |
| 5) COLLIMATOR 2B         | 18) EXIT WINDOW SUPPORT STRUCTURE                      |
| 6) ANTI-SCATTER BAFFLE   | 19) COLLIMATOR SUPPORT TUBE CENTERING RING             |
| 7) VACUUM CHAMBER        | 20) R VS. Z TRAJECTORIES OF PARTICLES                  |
| 8) MAGNET COIL           | EMITTED AT ANGLES $\alpha$ AND $\alpha_i \Delta\alpha$ |
| 9) VACUUM CHAMBER RING   | 21) FOCAL POINT REGION                                 |
| 10) RING FOCUS POSITION  | 22) LINE OF SIGHT BETA SHIELD                          |
| 11) EXIT WINDOW APERTURE |  |
| 12) MUHOENERGETIC BEAM   |  |
| 13) VACUUM CONNECTOR     |  |

Figure 1.1. Scale model of the Kansas State University magnetic lens monoenergetic electron source (KSU-MLMES#1). The ray traces depicted correspond to beta-particles emitted from the center face of a disk source with initial emission angles  $\alpha_i \Delta\alpha$ .

## II. THEORY OF OPERATION AND TERMINOLOGY

A beta-particle may be considered as a high energy electron originating from the decay of a neutron within the nucleus of a radioactive atom. A typical emission spectrum from a  $^{90}\text{Sr}/^{90}\text{Y}$  beta source is shown in fig. (2.1). The charge of a beta-particle is the same as that of an electron ( $q$ ). When a charged particle travels through a magnetic field ( $\vec{B}$ ) it experiences a magnetic force ( $\vec{F}_B$ ) as described by the Lorentz force equation

$$\vec{F}_B = q (\vec{v} \times \vec{B}) .$$

From the Lorentz force equation, observe that the magnetic force acts normal to the direction of particle motion. For this reason a magnetic field can do no work and hence cannot effect the energy of a charged particle. In addition, the magnetic force is directly proportional to the velocity and therefore energy of a particle. Because the magnetic force varies according to particle energy, particles of differing energies emitted in identical directions from a point source will be deflected along different trajectories.

Magnetic beta-particle spectrometers utilize the energy dispersing capability of a magnetic field coupled with a set of precisely positioned collimators to filter out all but a narrow range of particle energies. A magnetic lens spectrometer (MLS) is a widely used spectrometer configuration comprised of a cylindrical vacuum chamber with a magnet coil wound concentrically. A MLS can be converted into a source of monoenergetic electrons by simply constructing an exit window at the location normally occupied by the particle detector. This approach was followed by

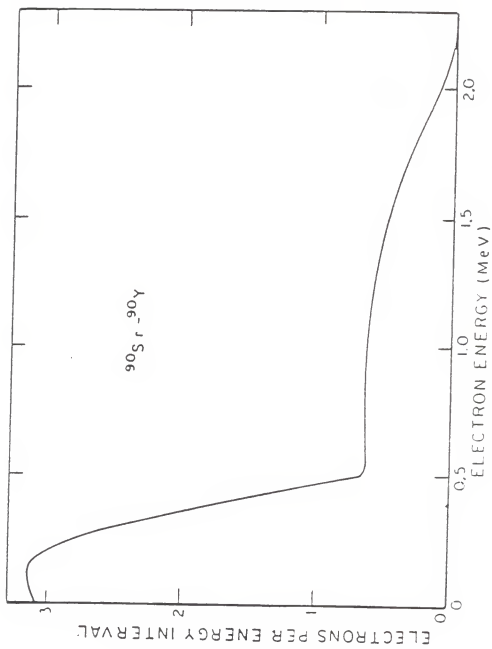


Figure 2.1. Typical beta spectrum from a  $^{90}\text{Sr}/^{90}\text{Y}$  source [10].

Graham and Elliot [9] and provides the basic concept upon which the KSU MLMES was designed. Figure (1.1) depicts the Kansas State University (KSU) concept—demonstrating magnetic lens monoenergetic electron source named appropriately (KSU-MLMES#1). Beta-particles emitted from a  $^{90}\text{Sr}/^{90}\text{Y}$  source located along the coil axis follow helical trajectories and focus in a region along the axis. In fig. (1.1) the radial component of the helical trajectories versus axial position of three particles of the same energy but emitted at angles  $\alpha$  and  $\alpha \pm \Delta\alpha$  are depicted. The particle traces shown are for particles emitted from the center of a disk source. The particle emitted at  $\alpha + \Delta\alpha$  just clears collimator 1a while the particle emitted at  $\alpha - \Delta\alpha$  just clears collimator 1b. A particle with initial emission angle  $\alpha$  traverses a path through the center of collimators 1a and 1b: the trajectory of a particle emitted at an angle  $\alpha$  is termed the central-ray trajectory.

From fig. (1.1) observe that the ray traces intersect one another in a narrow region termed the annular or point source ring focus position. Collimator sets 1 and 2 are positioned to coincide radially and axially with the point source ring focus position. The anti-scatter collimator is provided to eliminate vacuum chamber wall scattered particles from adding to the scattered component of the monoenergetic beam. The design of the exit window aperture also diminishes the scattered component of the beam as well as eliminates particles emitted from the source of incorrect energy from adding to the beam peak width.

Later sections in this thesis will document the design of each of the components of KSU-MLMES#1.

### III. VACUUM CHAMBER AND COIL DESIGN

The parameters governing the physical design of the vacuum chamber and coil are the central-ray initial emission angle, the maximum and minimum particle beam energies of interest, and the magnitude and shape of the focusing magnetic field. Typically the minimum energy particle of interest in beta dosimetry is 100 keV. The maximum beam energy of interest was selected to be approximately 2.3 MeV, corresponding to the maximum energy beta particle emitted by a  $^{90}\text{Sr}/^{90}\text{Y}$  beta-particle source.

### 3.1. SELECTION OF THE MAGNETIC FIELD SHAPE

Lindgren [11-13] summarized the resolution characteristics of several typical MLS axial field shapes as a function of initial emission angle. Figure (3.1) depicts the general results of his analysis. A qualitative comparison of the attributes of the field shapes relative to one another indicates that the field shapes labeled UF (uniform field), 24.5 (field strength in center decreases to 75% of the value at the source and detector), and 24 (source and detector are located at the ends of a solenoid) present superior resolution characteristics. Note that the field shape of the Lawrence National Laboratory MLMES is similar to the field shape labeled 8 or 13 in the figure.

Ideally a system using a uniform field shape would be selected. Uniform field MLS systems have been extensively analyzed due to the fact that they may be completely investigated analytically. The standard technique of obtaining a uniform field requires extending the length of the solenoidal coil a distance equal to 2 or 3 times the coil diameter beyond the source and focal points and by using additional end correcting coils. Unfortunately economical MLMES systems can't be constructed with a uniform field. This is a consequence of the fact that the coil in a uniform field MLMES would interfere with the conically shaped emitted beam.

Field shape 24 was selected over field shape 24.5 for the design of KSU-MLMES#1. MLMES systems utilize disk sources in order to obtain high monoenergetic beam intensities: for this reason the disk source resolution is the governing factor in selecting a field shape. Observe from fig. (3.1), to obtain equal disk source resolution, a system with field shape 24.5 requires larger initial emission angles than a system utilizing field shape 24. The initial emission angle is directly related to the physical size of a MLMES and therefore the amount of

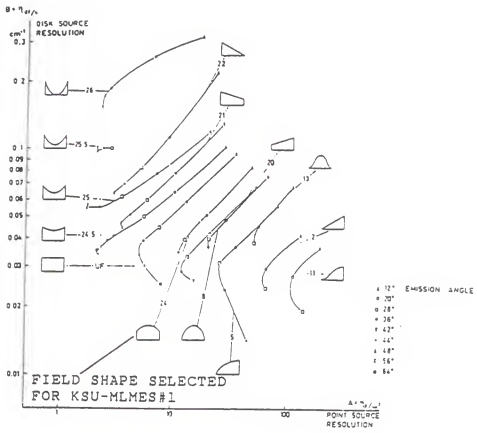


Figure 3.1. Resolution characteristics of several typical magnetic lens spectrometer field shapes as a function of the central-ray initial emission angle [11-13]. Field shape 24 was selected for the design of KSU-MLMES#1.



required materials (i.e. magnet wire and hence power-supply requirements, vacuum chamber size, etc.). Economic and performance considerations make a system based upon field shape 24 a reasonable choice.

### 3.2. SELECTION OF THE CENTRAL-RAY INITIAL EMISSION ANGLE

The economy and resolution of a system are each related to the magnitude of the central-ray initial emission angle. Generally as the angle increases the resolution improves; however, for reasons previously stated the economy of the system decreases. A trade off between resolution and economy was made leading to selection of a system based upon a central-ray initial emission angle of  $25^\circ$  even though fig. (3.1) clearly indicates improved resolution is obtainable at  $36^\circ$  for field shape 24.

In order to render the effect of the earth's magnetic field negligible, the minimum focusing magnetic field strength, (i.e. the field required to focus the minimum energy particles of interest (100 keV)), should be 100-150 times larger than that of the earth. The magnetic field of the earth is approximately  $5 \times 10^{-5}$  T [14], therefore the average magnetic focusing field strength for 100 keV particles should be  $\geq 7.5 \times 10^{-3}$  T.

### 3.3. DETERMINATION OF VACUUM CHAMBER DIMENSIONS

With the central-ray initial emission angle, and minimum values of kinetic energy and required focusing field specified, the diameter and pitch or "focal length" of the helical trajectory can be estimated based upon uniform field trajectory equations [6]

$$D = \frac{2m_0cs \sin(\alpha)}{qB} \sqrt{\left[\frac{E_k}{E_0} + 1\right]^2 - 1} \quad \left. \begin{array}{l} B = B_{\min} \\ E_k = E_{k_{\min}} \end{array} \right\} \quad (3.1)$$

$$L = \frac{2\pi m_0c \cos(\alpha)}{qB} \sqrt{\left[\frac{E_k}{E_0} + 1\right]^2 - 1} \quad \left. \begin{array}{l} B = B_{\min} \\ E_k = E_{k_{\min}} \end{array} \right\} \quad (3.2)$$

where: D = diameter of uniform field helical trajectory  
 L = focal length of uniform field helical trajectory  
 $\mu_0$  = permeability of vacuum  
 $m_0$  = rest mass of electron  
 c = speed of light in vacuum  
 q = charge of electron  
 B = magnetic field  
 $\alpha$  = central-ray initial emission angle  
 $E_k$  = kinetic energy of beta-particle  
 $E_0 = m_0c^2$  = rest mass energy of electron.

Note that the maximum diameter and focal length predicted by the uniform field equations are only approximations to the actual values for a MLMES utilizing a nonuniform field. The results of equations (3.1) and (3.2) indicated a trajectory of diameter 0.1259 m and of focal length 0.8483 m. The diameter of the vacuum

chamber must be greater than twice the diameter of the helical trajectory. refer to fig. (3.2).

Based upon these preliminary results, a vacuum chamber with inside diameter 0.254 m (10"), outside diameter 0.2794 m (11"), and length 1.016 m (40"), corresponding to an available standard size aluminum pipe, was selected.

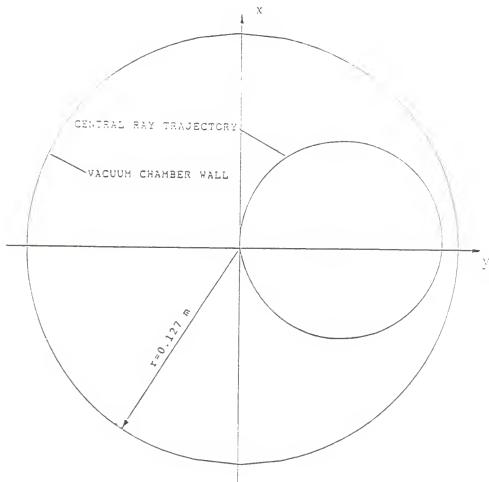


Figure 3.2. End-view of the vacuum chamber with the end-view of the central-ray trajectory inscribed. Note that the vacuum chamber diameter must be at least twice the maximum diameter of the end-view of the central-ray trajectory.

### 3.4. DESIGN OF THE MAGNET COIL

From eq. (3.1) and the trajectory diameter estimate, an average field of 0.0619 T was estimated to be required for focusing a particle of the maximum energy of interest (2.3 MeV). With the chamber outside diameter and required magnetic field range specified, the coil can be designed. Recall that for field shape 24, the source and focal points are positioned to correspond with the ends of the coil. The average value of the axial component of the magnetic field inside a coil of finite length and of narrow thickness is approximately, (refer to appendix B for derivation)

$$B_{z_{av}} = \frac{\mu_0 NI}{D^2} \left[ \sqrt{a^2 + D^2} - a \right] \quad (3.3)$$

where:  $\mu_0$  = permeability of vacuum  
N = number of turns in coil  
I = electric current flowing in the coil  
D = coil length  
a = effective coil radius: defined as  $(R_1+R_2)/2$ , where  
R<sub>1</sub> and R<sub>2</sub> are the inner and outer coil radii

For coil design purposes, a hypothetical coil was assumed of length equal to the focal length of the particle trajectory (0.8483 m) in order to yield field shape 24. The hypothetical coil was also assumed to have an effective radius of 0.1524 m (6"). Based on these estimations of the coil geometry, eq. (3.3) indicated that the product of the number of turns and the current would be  $6054 \leq NI \leq 49962$  corresponding to the required focusing fields for the minimum and maximum particle beam energies of interest. Either the number of turns or the maximum current rating for a selected wire gauge must be specified in order that both N and I can be determined. #6 A.W.G. varnish insulated aluminum magnet wire with a maximum current

rating of 50 A [15] was chosen. Based upon the maximum current rating of the wire, the required number of turns was found to be 1000.

The coil of KSU-MLMES#1 consists of 1196 turns of #6 A.W.G. aluminum magnet wire wound directly onto the vacuum chamber between two aluminum circular end rings. The actual coil is made up of a wire matrix of approximately 200 turns by 6 rows forming a coil with dimensions: length  $D=0.8509$  m (33.5"), inner radius  $R_1=0.1397$  m (5.5"), and outer radius  $R_2=0.16345$  m (6.435").

NOTE: the number of turns was increased from the estimate of 1000 to 1196. By increasing  $N$ , the required focusing current for the maximum energy particle of interest (2.3 MeV), will be beneficially decreased from the maximum current rating of the wire.

The magnetic field inside of KSU-MLMES#1 will be nonuniform with varying radial and axial field components between the source and detector. The next section will describe the derivation of the equations of motion for a particle traveling through the nonuniform field.

#### IV. THEORETICAL OPERATIONAL ANALYSIS

All aspects of the operation and performance of KSU-MLMES#1 must be performed numerically due to the nonuniform magnetic field utilized by the system. In the following sections we will first derive the equations of motion and magnetic flux-density vector at all points around a solenoidal coil. Next, the method used to solve the equations of motion will be presented followed by application of the numerical results to the design of the system. The design aspects that will be investigated are as follows:

- 1) determination of the range of allowed initial emission angles
- 2) determination of the source and focal point positions
- 3) determination of the spectrometer operating equation
- 4) determination of the point source ring focus position
- 5) determination of collimation angle
- 6) investigation of additional trajectory information and a comparison between numerical and approximate analytic solutions
- 7) determination of transmission and resolution characteristics of the system.



#### 4.1. DERIVATION OF THE EQUATIONS OF MOTION

The equations of motion are determined by examining the forces acting on a beta-particle as it travels through the nonuniform magnetic field of the MLMES. A magnetic force acts on the charged particle as given by the Lorentz equation

$$\vec{F}_B = q(\vec{v} \times \vec{B}). \quad (4.1)$$

In general, the velocity and magnetic field vectors will be functions of  $x$ ,  $y$  and  $z$  in rectangular coordinates

$$\begin{aligned} \vec{v} &= v_x \hat{x} + v_y \hat{y} + v_z \hat{z} \\ \vec{B} &= B_x \hat{x} + B_y \hat{y} + B_z \hat{z}. \end{aligned}$$

where  $\hat{x}$ ,  $\hat{y}$ , and  $\hat{z}$  are the rectangular coordinate system unit vectors. Substitution of the  $\vec{v}$  and  $\vec{B}$  vectors into the Lorentz force equation yields

$$\vec{F}_B = q[(v_y B_z - v_z B_y)\hat{x} + (v_z B_x - v_x B_z)\hat{y} + (v_x B_y - v_y B_x)\hat{z}]. \quad (4.2)$$

The magnetic force acting on the particle can be equated to Newton's 2nd law. Newton's 2nd law for a relativistic particle with constant speed is given as

$$\vec{F} = \tilde{m} \frac{d\vec{v}}{dt}, \quad (4.3)$$

where  $\tilde{m}$  is the moving mass of the particle. In rectangular coordinates the acceleration is given as

$$\frac{d\vec{v}}{dt} = \frac{dv_x}{dt} \hat{x} + \frac{dv_y}{dt} \hat{y} + \frac{dv_z}{dt} \hat{z}. \quad (4.4)$$

Substitution of eq. (4.4) into Newton's equation, followed by equating the vector components of the resulting expression to eq. (4.2) yields the equations of motion

$$\begin{aligned} \frac{dv_x}{dt} &= \frac{q}{\tilde{m}} (v_y B_z - v_z B_y) \\ \frac{dv_y}{dt} &= \frac{q}{\tilde{m}} (v_z B_x - v_x B_z) \\ \frac{dv_z}{dt} &= \frac{q}{\tilde{m}} (v_x B_y - v_y B_x). \end{aligned} \quad (4.5)$$

Note that the equations of motion are coupled. They are coupled since  $v_x$ ,  $v_y$  and  $v_z$  are interdependent upon one another and must therefore be solved simultaneously. Also note that  $B_x$ ,  $B_y$ , and  $B_z$  must be known at all points along the trajectory. In the next section the derivation of the magnetic field components will be provided.

## 4.2. DERIVATION OF THE MAGNETIC FLUX-DENSITY VECTOR

In this section, an accurate expression for evaluating the magnetic flux-density (field) vector at any point around the coil will be developed. The derivation of the field vector will be performed in rectangular coordinates for simplicity and then converted to cylindrical coordinates to make use of the system symmetry. The system configuration to be analyzed is depicted in fig. (4.1). An arbitrary point where the field is to be evaluated, i.e. the point (p,h) in cylindrical coordinates, is shown in the figure. Note the cylindrical symmetry of the system: the analysis can be simplified by considering the point (p,h) to lie in the xz plane without sacrificing generality. This is a direct consequence of the fact that a coil has only radial and axial magnetic field components, but no angular component. Two approximations are introduced to simplify the analysis:

Approximation 1) the coil volume consists of a close-packed matrix of conductor, insulation, and air gaps: a uniform current density is assumed to flow through the entire cross sectional area of the coil. The current-density magnitude, having units of A/m<sup>2</sup>, is given by

$$J = \frac{NI}{A}, \quad (4.6)$$

where: N = number of turns in the coil  
I = electric current  
A = cross sectional area of coil.

The coil side-view cross sectional area is given as

$$A = D(R_2 - R_1), \quad (4.7)$$

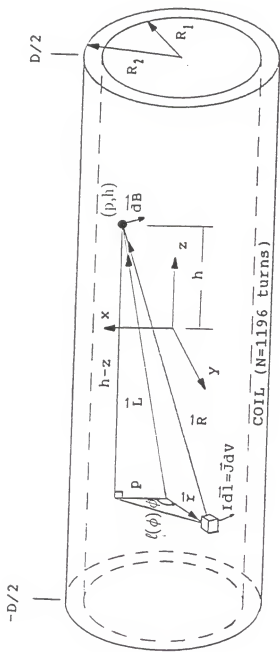


Figure 4.1. Geometry of the coil utilized in evaluating the magnetic flux-density vector. The differential magnetic field strength ( $d\vec{B}$ ) at the point  $(p, h)$  generated by a differential current element ( $\vec{J}dv$ ) is depicted.

where:  $D$  = length of coil  
 $R_1$  = inner radius of coil  
 $R_2$  = outer radius of coil.

Approximation 2) The pitch of individual turns in the winding are neglected.

Note that the first approximation converts the problem of evaluation of the field at a point from one of summing the field contribution at the point from each individual turn in the coil to one of integration over the volume occupied by all turns in the coil.

The differential form of the Biot-Savart law relates the differential magnetic field vector at a point, say  $(p,h)$  in cylindrical coordinates, to a differential current element generating the field:

$$d\vec{B}(p,h) = \frac{\mu_0}{4\pi R^2} (I d\vec{l} \times \hat{R}) = \frac{\mu_0}{4\pi R^3} (I d\vec{l} \times \vec{R}),$$

where  $\hat{R} \equiv \vec{R}/R$ . To obtain the magnetic field vector at the point  $(p,h)$ , we simply integrate the differential form of the Biot-Savart law over the coil volume:

$$d\vec{B} = \frac{\mu_0}{4\pi} \int \int \int_{\text{coil volume}} \frac{\vec{J}(\vec{r}) \times \vec{R}}{R^3} dV, \quad (4.8)$$

where we have used the relation  $I d\vec{l} = \vec{J}(\vec{r}) dV$ ;  $dV$  being the differential volume element and  $\vec{J}(\vec{r})$  is the current density vector that will be described later. The task at hand becomes one of defining each quantity in the integral form of the Biot-Savart law. Each of the quantities defined in fig. (4.1) is instrumental in developing the terms of the Biot-Savart law and will be described below.

$\vec{L} \equiv$  variable position vector of the point (p,h), where the field is to be calculated, with respect to the transverse plane containing the current element:  $\vec{L}$  is given as

$$\vec{L} = p\hat{x} + (h-z)\hat{z} .$$

$\vec{r} \equiv$  variable vector defining the radial and angular position of the current element and is given as

$$\vec{r} = r\cos(\phi)\hat{x} + r\sin(\phi)\hat{y} .$$

$\ell(\phi) \equiv$  magnitude of the line segment connecting the projection of the point (p,h) into the xy plane containing the differential current element, and the differential current element. Note that the magnitude of  $\ell$  varies with angle  $\phi$  and is obtained by applying the law of cosines to the triangle in the xy plane containing the differential current element as an apex

$$\ell(\phi) = \sqrt{r^2 + p^2 - 2rp\cos(\phi)} .$$

$\vec{R} \equiv$  variable vector pointing from the differential current element to the point (p,h): by vector addition  $\vec{R}$  is given as

$$\vec{R} = \vec{L} - \vec{r} = (p-r\cos(\phi))\hat{x} - r\sin(\phi)\hat{y} + (h-z)\hat{z} . \quad (4.9)$$

$R \equiv$  variable magnitude of  $\vec{R}$ : one way of deriving  $R$  is from the Pythagorean theorem

$$R = \sqrt{[\ell(\phi)]^2 + (h-z)^2}.$$

Substitution of  $\ell(\phi)$  into the expression for  $R$  yields

$$R = \sqrt{r^2 + p^2 + (h-z)^2 - 2rp\cos(\phi)},$$

where  $h-z \equiv$  variable axial separation distance between the current element and point  $(p, h)$ .

$\vec{J}(\vec{r}) \equiv$  variable current density vector; earlier the magnitude was presented in eq. (4.6). The direction is obtained by noting that  $\vec{J}(\vec{r})$  is perpendicular to  $\vec{r}$  or else by noting  $\vec{J}(\vec{r})$  is in the same direction as the cylindrical coordinate unit vector  $\hat{\phi}$ : i.e. namely,  $-\sin(\phi)\hat{x} + \cos(\phi)\hat{y}$ . Therefore the current density vector is

$$\vec{J}(\vec{r}) = \frac{NI}{D(R_2 - R_1)} (-\sin(\phi)\hat{x} + \cos(\phi)\hat{y}).$$

The cross product between  $\vec{J}(\vec{r})$  as given in the previous expression and  $\vec{R}$  as given in eq. (4.9) yields

$$\vec{J}(\vec{r}) \times \vec{R} = \cos(\phi)(h-z)\hat{x} + \sin(\phi)(h-z)\hat{y} + (r - p\cos(\phi))\hat{z}.$$

Next a conversion to the cylindrical coordinates system is desired because the magnetic field only has two components, i.e. a radial and axial component, in the cylindrical coordinate system. In general the coordinate transformation equations are

$$\begin{aligned}\hat{r} &= \cos(\phi)\hat{x} + \sin(\phi)\hat{y} \\ \hat{\phi} &= -\sin(\phi)\hat{x} + \cos(\phi)\hat{y} \\ \hat{z} &= \hat{z} ;\end{aligned}$$

however, we must specifically apply the transformations at the point (p,h) at which  $\phi=0$ . For this reason the correct coordinate transformations are given as

$$\begin{aligned}\hat{r} &= \hat{x} \\ \hat{\phi} &= \hat{y} \\ \hat{z} &= \hat{z} .\end{aligned}$$

Therefore, we obtain

$$\vec{J}(\vec{r}) \times \vec{R} = \cos(\phi)(h-z)\hat{r} + \sin(\phi)(h-z)\hat{\phi} + (r - p\cos(\phi))\hat{z} . \quad (4.11)$$

In cylindrical coordinates the differential volume is given as

$$dV = r dr d\phi dz . \quad (4.12)$$

Now all required quantities are known and can be substituted into the integral form of the Biot-Savart law. Substitution of equations (4.10), (4.11) and (4.12) into eq. (4.8) yields

$$B(p,h) = \frac{\mu_0 NI}{4\pi D(R_1 - R_2)} \int_{z=-D/2}^{D/2} \int_{\phi=0}^{2\pi} \int_{r=R_1}^{R_2} \frac{r(h-z)[\cos(\phi)\hat{r} + r(h-z)\sin(\phi)\hat{\phi} - r(p\cos(\phi)-r)\hat{z}]}{[r^2 + p^2 + (h-z)^2 - 2rp\cos(\phi)]^{3/2}} dr d\phi dz$$



Integration over the coil volume is over cylindrical coordinates  $r, \phi, z$ . To avoid confusion, note that the radial and axial position of the particle in cylindrical coordinates are denoted as  $(p, h)$ . The  $\phi$  term integrates analytically to zero leaving only a radial and axial component as expected. Integration over coil length was performed analytically leaving the radial and axial magnetic field vector components in the form

$$B_r(p, h) = \frac{\mu_0 NI}{4\pi D(R_2 - R_1)} \int_{\phi=0}^{2\pi} \int_{r=R_1}^{R_2} \cos(\phi) \left[ \frac{1}{\sqrt{r^2 + p^2 + (h-D/2)^2 - 2rp\cos(\phi)}} - \frac{1}{\sqrt{r^2 + p^2 + (h+D/2)^2 - 2rp\cos(\phi)}} \right] dr d\phi$$

$$B_z(p, h) = \frac{\mu_0 NI}{4\pi D(R_2 - R_1)} \int_{\phi=0}^{2\pi} \int_{r=R_1}^{R_2} \frac{r(\cos(\phi) - r)}{r^2 + p^2 - 2rp\cos(\phi)} \left[ \frac{(h - D/2)}{\sqrt{r^2 + p^2 + (h-D/2)^2 - 2rp\cos(\phi)}} - \frac{(h + D/2)}{\sqrt{r^2 + p^2 + (h+D/2)^2 - 2rp\cos(\phi)}} \right] dr d\phi$$

where:

- (p, h) = radial and axial coordinates of position where field is to be evaluated (h measured from center of coil)
- N = number of turns in coil
- I = electric current flowing in coil
- D = length of the coil
- R<sub>1</sub> = inner radius of coil
- R<sub>2</sub> = outer radius of coil
- μ<sub>0</sub> = permeability of vacuum
- φ = angular variable of integration over coil volume
- r = radial variable of integration over coil volume.

A FORTRAN code named FIELD was written which utilized 16-point double Gauss-Quadrature numerical integration to determine the field components at any specified point (p, h): (the source code listing is provided in appendix A). Several plots of the individual field components are provided on the following pages to demonstrate the characteristics of the magnetic field around the coil. The next section will cover the topic of solving the nonlinear coupled equations of motion.

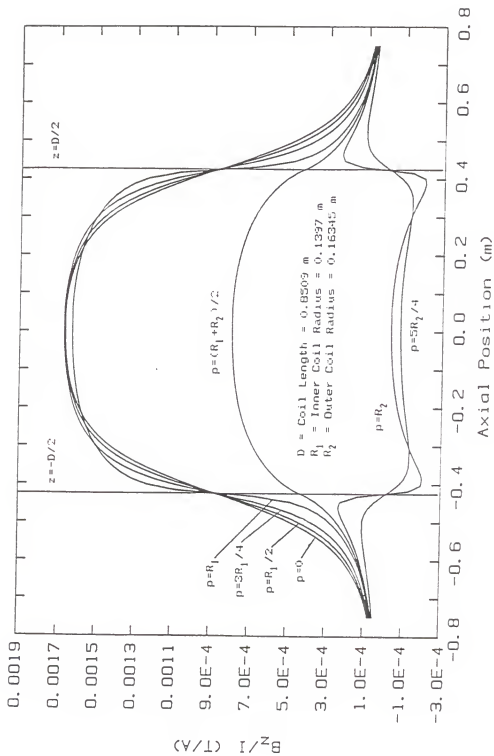


Figure 4.2. Shape of the axial component of the magnetic field along the solenoid at several radial positions. Division of  $B_z$  by the electric current ( $I$ ) yields relative field shape information that is only a function of the physical geometry of the coil.



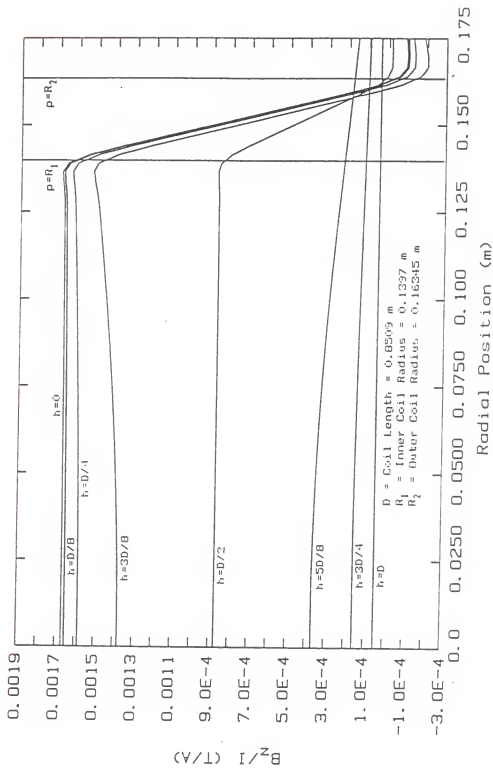


Figure 4.4. Transverse shape of the axial component of the magnetic field at several axial positions.

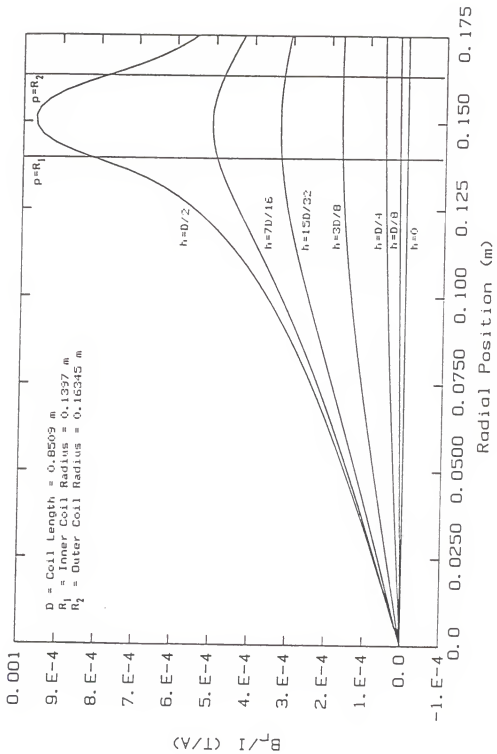


Figure 4.5. Transverse shape of the radial component of the magnetic field at several axial positions.

#### 4.3. SOLUTION OF THE EQUATIONS OF MOTION

The equations of motion were presented in eq. (4.5). An accurate solution of the equations of motion can only be performed numerically. The Runge-Kutta 4th order (RK4) numerical method was implemented in the solution of the equations for its ease of application and accuracy. Recall that the equations of motion were expressed as first order ordinary differential equations in terms of the rectangular velocity components:  $v_x$ ,  $v_y$ , and  $v_z$ . The helical trajectory, given in rectangular coordinates as  $x$ ,  $y$  and  $z$  as functions of time or axial position, is the desired solution. The velocity is simply the time rate of change of position, therefore the equations of motion can be expressed as the following set of first order ordinary differential equations:

$$\frac{dv_x}{dt} = \frac{q}{\tilde{m}} (v_y B_z - v_z B_y)$$

$$\frac{dv_y}{dt} = \frac{q}{\tilde{m}} (v_z B_x - v_x B_z)$$

$$\frac{dv_z}{dt} = \frac{q}{\tilde{m}} (v_x B_y - v_y B_x)$$

$$\frac{dx}{dt} = v_x$$

$$\frac{dy}{dt} = v_y$$

$$\frac{dz}{dt} = v_z$$

Six initial conditions are required: one for each 1st order equation. The initial position and velocity components of the particle yield the required initial conditions.

A FORTRAN program named (PATH-RK4) was written to solve the equations of motion in rectangular coordinates, (refer to appendix A for self-explanatory source-code listing). The program is general in nature and can be used to design new or analyze any existing MLS system that has a single rectangularly shaped coil. A brief description of the required input data, logic, and the output data generated by the program will be provided:

#### REQUIRED INPUT DATA

- 1) coil geometry: coil length (m)  
inner coil radius (m)  
outer coil radius (m)  
# turns in coil
- 2) vacuum chamber inside radius and length (m)
- 3) source location  $[x(0),y(0),z(0)]$  (m)
- 4) electric current flowing through the coil (A)
- 5) particle kinetic energy (MeV)
- 6) initial emission angle with respect to axial direction (degrees)
- 7) trajectory convergence option
  - 1) track the particle until it reaches the focal point: the focal point is defined as the axial position at which the trajectory reaches a minimum radial value
  - 2) track the particle until it reaches a user defined axial position

#### LOGIC

- 1) step particle forward in time along the trajectory by using the RK4 numerical routine to solve the equations of motion
- 2) evaluate the radial and axial magnetic field components at each point and horner along the trajectory as required

- 3) test for particle convergence: a particle is considered to have converged when its trajectory reaches a minimum radial value or when it reaches a user defined axial position

#### OUTPUT DATA

- 1) radial and axial components of the magnetic field acting upon the particle versus the particle's axial position,  $z$
- 2) velocity components  $v_x$ ,  $v_y$ , and  $v_z$  versus  $z$
- 3) the helical trajectory is 3-dimensional: the  $x,y,z$  coordinates of the point obtained at each time step along the trajectory are provided
- 4) useful design characteristics of the trajectory are readily obtained by considering 2-dimensional views of the trajectory: the following data files are generated:
  - a) trajectory rectangular coordinate:  $x$  versus  $z$
  - b) trajectory rectangular coordinate:  $y$  versus  $z$
  - c) trajectory cylindrical coordinate:  $r$  versus  $z$
  - d) trajectory end view in rectangular coordinates:  $x$  versus  $y$
- 5) trajectory focal length: defined as source to focal point distance.

Output data from the program were used to specify the source and focal point locations, position of ring focus, required angle of collimator edges, the spectrometer operating equation, and the theoretical resolution of the system. A discussion of the determination of each of these design specifications will be provided in the following sections; but first the determination of the range of allowed initial emission angles will be presented to clarify the discussion that follows.

#### 4.3.1. DETERMINATION OF THE RANGE OF INITIAL EMISSION ANGLE

Only particles emanating from the source into a prescribed range of initial emission angles ( $\alpha \pm \Delta\alpha$ ), with respect to the MLMES axis, will be allowed to pass through the first collimator. The range of allowable initial emission angles about



the central-ray initial emission angle ( $\alpha$ ) depends upon the desired transmission (T). Recall that transmission is defined as the fraction of the particles of selected energy emitted by a point source that are allowed to pass through the first collimator. The usable fraction of the total solid angle is given as

$$4\pi T = \int_{\theta=\alpha-\Delta\alpha}^{\alpha+\Delta\alpha} 2\pi\sin(\theta)d\theta.$$

The integration yields

$$4\pi T = -2\pi[\cos(\alpha+\Delta\alpha) - \cos(\alpha-\Delta\alpha)].$$

Use of the trigonometric identity

$$\sin(\beta) \sin(\gamma) = \frac{1}{2} [\cos(\beta-\gamma) - \cos(\beta+\gamma)],$$

yields

$$T = \sin(\alpha) \sin(\Delta\alpha).$$

Solve for the only unknown  $\Delta\alpha$  and obtain

$$\Delta\alpha = \sin^{-1} \left[ \frac{T}{\sin(\alpha)} \right].$$

The range of allowed initial emission angles for 1.0% transmission is  $25^\circ \pm 1.356^\circ$  and  $25^\circ \pm 0.678^\circ$  for 0.5% transmission. Knowledge of the range of initial

emission angles plays an important role in determining the source, focal point, ring focus and collimator positions as will become apparent in the sections that follow.

#### 4.3.2. DETERMINATION OF THE SOURCE AND FOCAL POINT POSITIONS

Recall from the COIL AND VACUUM CHAMBER DESIGN section that an estimate of the focal length was calculated based upon uniform field expressions for the helical trajectory. In order to determine the required actual focal length, the program PATH-RK4 was run using the actual coil and vacuum chamber dimensions. For KSU-MLMES#1, the maximum focal length of particles emitted at the central-ray initial emission angle ( $\alpha=25^\circ$ ), is approximately 0.8141 m. At this focal length the source is located at (0,0,-0.40705 m) and a 3.0565 MeV particle, at a focusing current of 50 A, will symmetrically focus while just clearing the vacuum chamber wall, refer to fig. (4.6). The actual focal length was reduced to 0.762 m to prevent particles emitted from a point source at the maximum allowed angle of  $26.356^\circ$  (corresponding to a 1% transmission configuration from a point source) from striking the vacuum chamber wall is provided to account for a small disk rather than point source. At a focal length of 0.762 m, a 2.83686 MeV particle will symmetrically focus when a focusing current of 50 A is applied to the coil.

In summary, the following design specifications were found in this section:

- 1) source axial position:  $z=-0.381$  m
- 2) central ray focal point position:  $z=+0.381$  m
- 3) at the maximum current of 50 A, the maximum energy particle that can be focused by the MLMES for a focal length of 0.762 m is 2.83686 MeV.

In the next section the spectrometer operating equation will be developed.

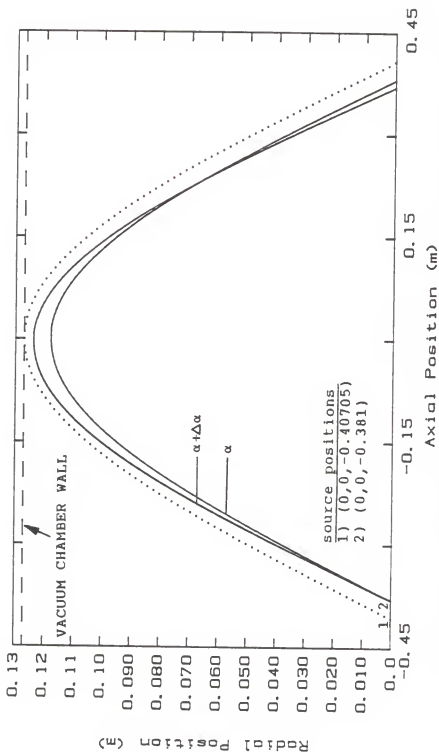


Figure 4.6. Ray traces for a variety of source positions that were examined to determine appropriate source position. Source position:  
 1) maximum at which central-ray symmetric focusing occurs, and  
 2) selected source position.

#### 4.3.3. DETERMINATION OF THE SPECTROMETER OPERATING EQUATION

The spectrometer operating equation stipulates the kinetic energy of the particle that will be focused for a given electric current flowing through the MLMES coil. A focused particle is defined according to the following criterion: 1) initial emission angle of  $25^\circ$ , 2) emitted from the front center face of the disk source at the point (0,0,-0.381 m), and 3) must focus at an axial position of  $z=0.381$  m.

The program PATH-RK4 was run with input data: source point (0,0,-0.381), initial emission angle  $25^\circ$ , an electric current was selected and a kinetic energy was assumed. After each run the focal length generated by PATH-RK4 was compared to 0.762 m. The assumed kinetic energy was lowered if the focal length obtained was greater than 0.762 m and raised otherwise. This iterative process continued to convergence. Results of this analysis are tabulated below.

Table 4.1. The kinetic energy of particles that will be focused for a specified electric current. The data was generated by an iterative application of the program PATH-RK4.

Electric Current (A)	Focused Kinetic Energy (MeV)	Focal Length (m)
0.0	0.0	undefined
3.0	0.03721	0.7620430
10.0	0.32506	0.7619963
20.0	0.90768	0.7620029
30.0	1.53889	0.7620006
40.0	2.18478	0.7620012
50.0	2.83686	0.7620011

A plot of the data in table (4.1) is presented in fig. (4.7). The shape of the resulting curve appears to be characteristic of spectrometers in general. (i.e. note the curved tail at low kinetic energies and currents and nearly linear response at

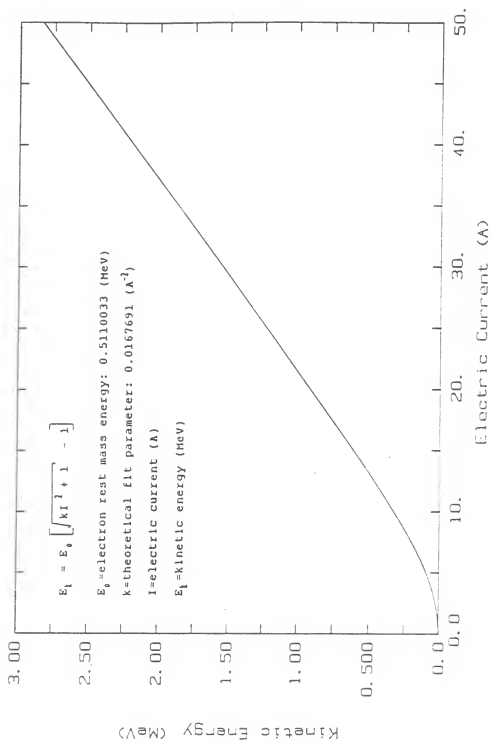


Figure 4.7. Plot of the spectrometer operating equation. The figure depicts the kinetic energy of the monoenergetic beam that will be emitted by KSU-MUES#1 for a given electric current.

higher energies and currents). In the case of uniform field MLS systems an analytic expression relating the particle energy and the corresponding focusing current can be derived from equation (3.1) or (3.2). The resulting expression will be referred to as the spectrometer operating equation and is of form

$$E_k = E_o \left[ \sqrt{kI^2 + 1} - 1 \right] \quad (4.13)$$

where:  $E_k$  = kinetic energy (MeV)  
 $E_o$  = electron rest mass energy (MeV)  
 $I$  = electric current (A)  
 $k$  = constant =  $[qRB/(m_o c I \sin(\alpha))]^2 = [qLB/(2\pi m_o c I \cos(\alpha))]^2$

For uniform field MLS systems the physical quantities making up the constant  $k$  are electric charge ( $q$ ), radius of curvature ( $R$ ), magnetic field ( $B$ ), electron rest mass ( $m_o$ ), speed of light ( $c$ ), electric current ( $I$ ), and the sine of the angle between the velocity and magnetic field vectors ( $\sin(\alpha)$ ), when equation 3.1 is used to derive the spectrometer operating equation. If equation 3.2 is used to derive the spectrometer operating equation the different quantities making up the constant  $k$  include the pitch or "focal length" ( $L$ ), and the cosine of the angle between the velocity and magnetic field vectors ( $\cos(\alpha)$ ). Equation (4.13) also applies to nonuniform field systems except average values of the radius of curvature, magnetic field and sine of the angle between the velocity and magnetic field vectors are used. Note that  $k$  is a constant because the average radius of curvature and average value of  $\sin(\alpha)$  are independent of kinetic energy. Further the ratio of the average value of the magnetic field divided by the electric current is simply a constant relating to the coil geometry. Rather than determining the average values of  $R$ ,  $B/I$ , and  $\sin(\alpha)$  for the central ray trajectory, the parameter  $k$  was simply treated as a constant curve

fit parameter that was evaluated by substituting in one of the data points from table 4.1. The point  $I=50$  A and  $E_k=2.83686$  MeV was arbitrarily selected yielding a value of the parameter  $k=0.0167691$  A<sup>-2</sup>.

In summary, the spectrometer operating equation predicts the peak energy of the monoenergetic beam that will be emitted from the MLMES for a specified electric current. The equation was found to be

$$E_k = 0.5110033 \left[ \sqrt{0.0167691 I^2 + 1} - 1 \right].$$

#### 4.3.4. DETERMINATION OF THE POINT SOURCE RING FOCUS POSITION

From fig. (4.8), the  $r$  versus  $z$  trajectories of particles of selected energy emitted at  $\alpha$  and  $\alpha \pm \Delta\alpha$  (corresponding to 1% transmission) are observed to intersect one another in a narrow region known as the annular or point source ring focus position. It is common practice to locate the second collimator where the intersecting traces have minimum width. A magnified view of the trajectory intersection region is provided in figure (4.9). From a further magnified view the point of minimum width (ring focus position) was graphically determined to be approximately  $r=0.0628$  m and  $z=0.2406$  m.

#### 4.3.5. DETERMINATION OF COLLIMATION ANGLE

The angle that the central-ray trajectory makes with respect to the axial direction at the ring focus position is defined as the collimation angle. It is important to know the collimation angle since it corresponds to the angle at which the collimator surfaces must be beveled. A linear slope fit was performed using ( $r,z$ ) data points on either side of the ring focus point resulting in an angle of 22.3°.

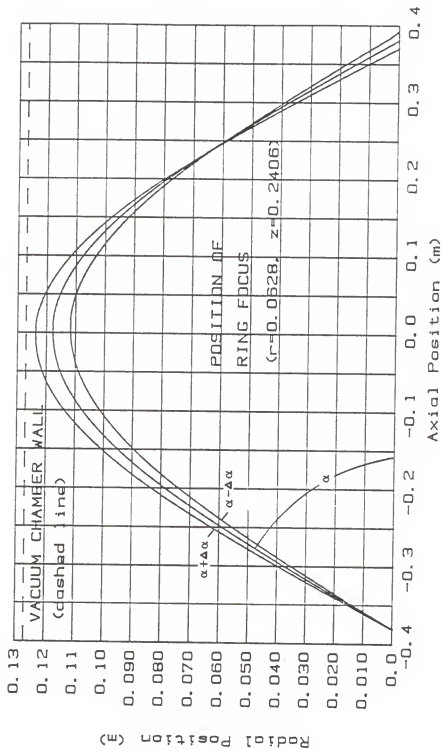


Figure 4.8. The radial component of the helical trajectory versus axial position of particles emitted from a point source at angles  $\alpha \pm \Delta\alpha$  (corresponding to 1% transmission). The figure clearly indicates the annular focusing that is typical of magnetic lens spectrometer systems.



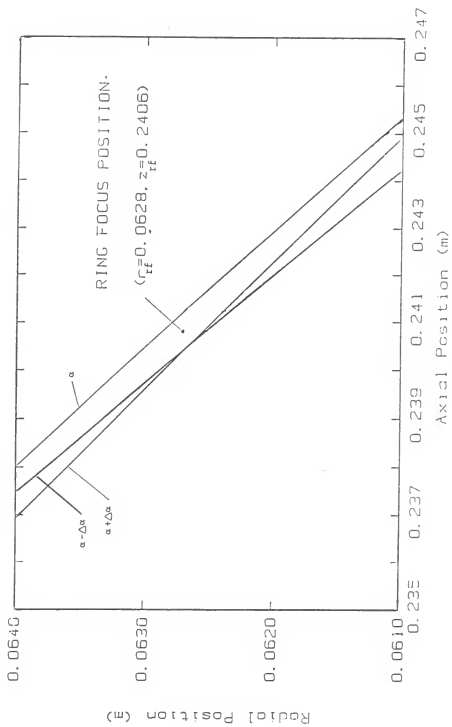


Figure 4.9. Magnified view of the point source ring focus position.

#### 4.3.6. ADDITIONAL TRAJECTORY INFORMATION GENERATED BY PATH-RK4

The program PATH-RK4 is a versatile program that generates a tremendous amount of useful information. The design of the MLMES was primarily based upon analysis of  $r$  vs.  $z$  ray traces. Additional information provided by the program includes rectangular coordinates of points  $(x,y,z)$  along the helical trajectory, the radial and magnetic field components that a beta-particle experiences as it travels through the MLMES, and the velocity components of the particle in rectangular coordinates  $(v_x,v_y,v_z)$  as it travels through the MLMES. Figure (4.10) shows the energy independent central ray trajectory ray trace  $r$  vs.  $z$  as well as the rectangular components of the ray trace ( $x$  and  $y$  vs.  $z$ ). Figures (4.11) and (4.12) represent the relative shape of the radial and axial magnetic field components that a particle will experience as it travels along the central ray trajectory through the MLMES. Note the vertical axis of each plot is  $B_r/I$  and  $B_z/I$  rather than  $B_r$  and  $B_z$  as generated by the program. The plots were presented in this manner since they yield energy independent relative magnetic field shape information that is only a function of the coil geometry. Figure (4.13) indicates typical velocity components of a 1 MeV particle as it travels along the central-ray trajectory. The velocity components will have the same general shape but will be of different magnitude for particles of different energies traveling along the central-ray trajectory.

In addition the end-view of the helical trajectory may be generated by plotting the  $x$  versus  $y$  components of data points along the helical trajectory. refer to fig. (4.14). An unexpected observation was made regarding the end-view of the helical central-ray trajectory. Intuitively one would expect that a particle emitted from a point along the axis into the  $xz$  plane would follow a trajectory symmetric with respect to the  $yz$  and  $z=0$  planes for a magnetic field symmetric about the  $z=0$

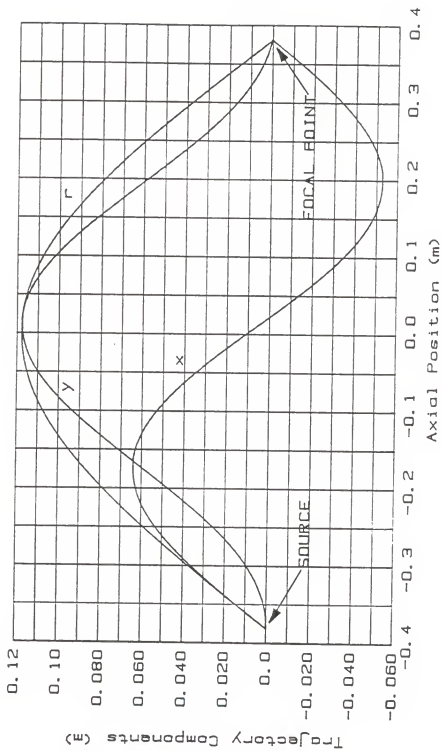


Figure 4.10. Central-ray trajectory versus axial position in rectangular and cylindrical coordinates. Note that the  $r$  vs.  $z$  trace is symmetric about the plane  $z=0$ ; however, the individual rectangular components making up  $r$  (i.e.  $x$  and  $y$ ) are not symmetric.

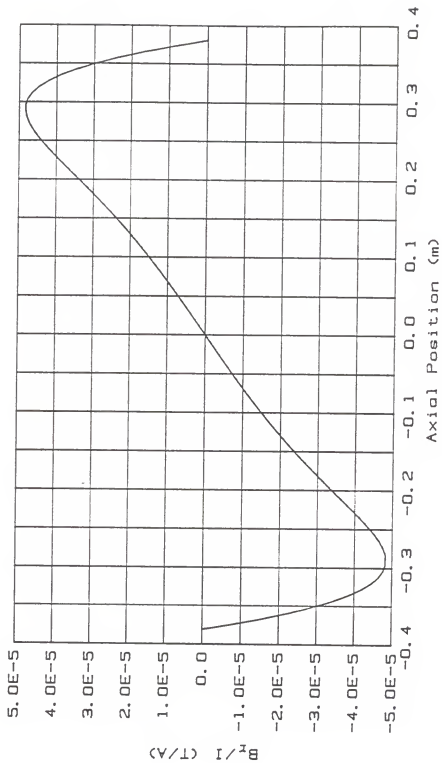


Figure 4.11. Shape of the radial component of the magnetic field experienced by a beta-particle as it travels along the central-ray trajectory.  $B_r$  is divided by the electric current (I) to yield relative field shape information that is independent of particle energy.

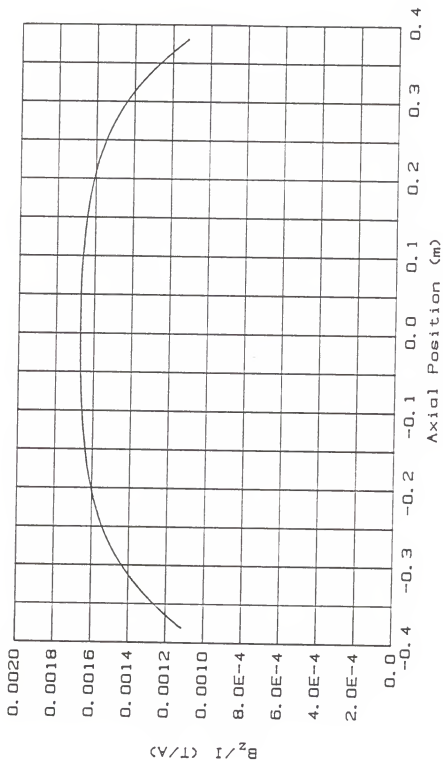


Figure 4.12. Shape of the axial component of the magnetic field experienced by a beta-particle as it travels along the central-ray trajectory.  $B_z$  is divided by the electric current (I) to yield relative field shape information that is independent of particle energy.

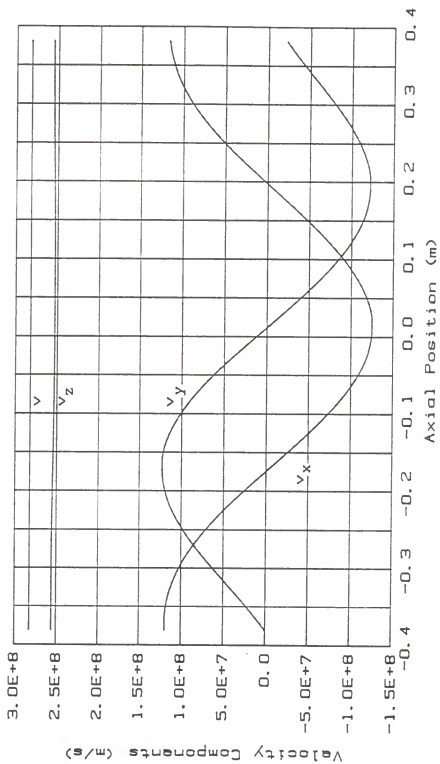


Figure 4.13. Rectangular velocity components of a 1 MeV beta-particle traveling along the central-ray trajectory. Note that the velocity components at the focal point are not the same as at the source point.

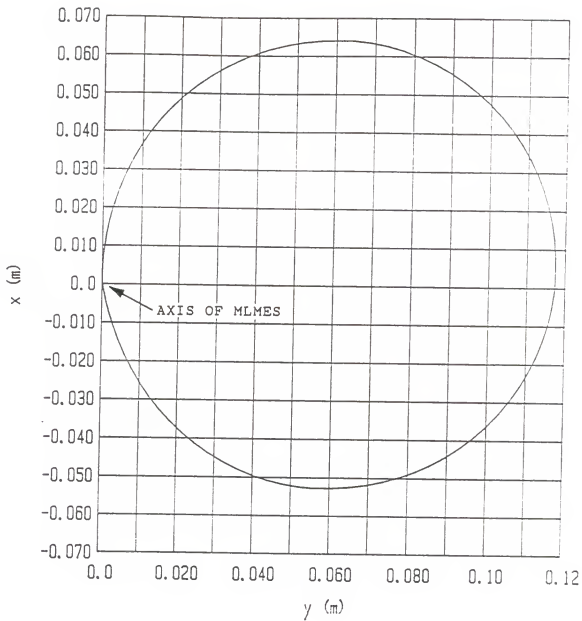


Figure 4.14. Two dimensional ( $x$  vs.  $y$ ) end-view of the central-ray trajectory. Note the distinctly unsymmetric end-view about the  $yz$  plane: ( $z$  into the page).

plane. However, fig. (4.14) clearly indicates that the expected symmetry does not exist. The dilemma was resolved by demonstrating that the analytic solution to a simplified form of the equations of motion yielded an unsymmetric end-view offset in the same manner as the numerical solution. The analytic solution will not be provided; however, the simplifying approximations required to reduce the problem to an extent that an analytic solution can be obtained and the analytic results will be provided to demonstrate the correctness of the numerical solution.

#### REQUIRED APPROXIMATIONS

Approximation 1) The radial component of the magnetic field must be neglected in order to solve the equations of motion analytically.

Approximation 2) The axial component of the magnetic field throughout the volume between the source and focal points was assumed to be described by the value along the axis of a solenoid of finite length, namely

$$B_z(z) = \frac{\mu_0 NI}{2D} \left[ \frac{(z+D/2)}{\sqrt{a^2+(z+D/2)^2}} - \frac{(z-D/2)}{\sqrt{a^2+(z-D/2)^2}} \right],$$

where:

- $\mu_0$  = permeability of vacuum
- $N$  = number of turns in coil
- $I$  = electric current flowing in the coil
- $D$  = length of coil
- $a$  = effective radius of coil  $(R_1+R_2)/2$ :  $R_1$  and  $R_2$  being the inner and outer coil radii respectively
- $z$  = axial position where the field is to be evaluated.



## OBSERVATIONS AND RESULTS FROM THE ANALYTIC SOLUTION

- Observation 1) The end-view predicted by the analytic solution is unsymmetric and is shifted in the same manner predicted by the numerical solution.
- Observation 2) The velocity components of the particle at the focal point will not be the same as they were at the source. The analytic solution indicated that  $v_y$  would be negative at the focal point rather than zero as it is at the source point,  $v_x$  would be positive but decreased in magnitude at the focal point relative to the source point, and  $v_z$  would be the same at the focal point as the source point. Figure (4.13) clearly indicates that the numerical solution displays these characteristics. The speed of the particle will remain constant along the trajectory as required.
- Observation 3) The analytic solution indicated that the  $r$  versus  $z$  ray trace would be symmetric about the  $z=0$  plane, while the  $x$  and  $y$  components making up  $r$  would not be symmetric about the plane  $z=0$ . Again, the numerical solution presented in fig. (4.10) clearly displays the trends predicted by the analytic solution.

#### 4.4. DETERMINATION OF TRANSMISSION AND RESOLUTION CHARACTERISTICS

The resolution of a MLMES depends on the selected transmission, monoenergetic beam energy, and disk source diameter. In this section, the effect each of these parameters has on the base-width resolution will be examined. In general the resolution also depends on the source spectrum, selected central-ray initial emission angle, and magnetic field shape. The base width resolution is defined as

$$R_b = \frac{\Delta E_k}{E_{k\text{selected}}} = \frac{E_{k\text{max}} - E_{k\text{min}}}{E_{k\text{selected}}},$$

where the maximum and minimum energy particles that contribute to the beam define the peak base-width. The following process was followed to determine  $E_{k\text{max}}$ ,  $E_{k\text{min}}$ , and the base-width resolution:

- 1) The axial positions of collimators 1a and 1b were determined for 1% and 0.5% transmissions. Recall that the range of initial emission angles is  $25 \pm 1.356^\circ$  and  $25 \pm 0.678^\circ$  for 1% and 0.5% transmission respectively. Collimators 1a and 1b are positioned radially to correspond with the ring focus radial position ( $r_{\text{rf}}=0.0628$  m). They are positioned axially to correspond with  $r$  versus  $z$  ray traces  $\alpha \pm \Delta\alpha$ . For 1% transmission the axial position of collimator 1a is  $z_{1a}=-0.2498$  m and for collimator 1b is  $z_{1b}=-0.231$  m, while for 0.5% transmission:  $z_{1a}=-0.2455$  m and  $z_{1b}=-0.2361$  m, refer to fig. (4.15). The axial collimator positions were obtained by performing a linear interpolation on the  $r$  versus  $z$  data for ray traces  $\alpha \pm \Delta\alpha$  about  $r_{\text{rf}}$ .

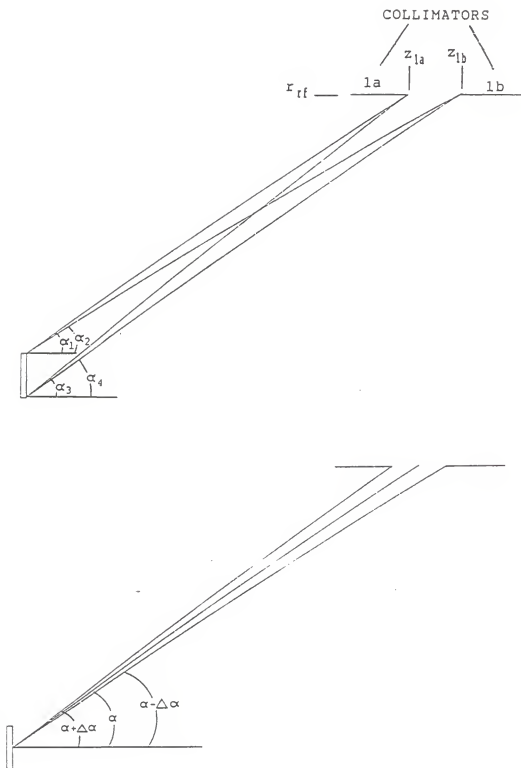


Figure 4.15.  $r$  versus  $z$  ray traces for particles of selected energy emitted at extremum angles  $\alpha_1, \alpha_2, \alpha_3, \alpha_4$  and from the center of a disk source at  $\alpha$  and  $\alpha \pm \Delta\alpha$ .

- 2) Figure (4.15) depicts particles of selected energy emitted at extremum angles from the periphery of a disk source of radius ( $r_{\text{disk}}$ ), and particles of selected energy emitted at  $\alpha$  and  $\alpha \pm \Delta\alpha$  from the front center face of the disk source. In each case the angle denoted is for a particle of selected energy that will just clear collimator 1a or 1b as shown. Angles  $\alpha_1$ ,  $\alpha_2$ ,  $\alpha_3$ , and  $\alpha_4$  must be determined because the maximum and minimum particle energies that contribute to the beam and the axial position of collimators 2a and 2b are determined by tracking particles emitted at these angles. Extremum angles  $\alpha_1$  and  $\alpha_3$  were found by emitting particles of selected energy at angles greater than and less than each angle from source positions ( $\pm r_{\text{disk}}, 0, -0.381$ ) respectively. The radial value of each  $r$  versus  $z$  ray trace at the axial position of collimator 1a was recorded and a linear interpolation was performed about  $r_{\text{rf}}$  yielding the desired extremum angles. Extremum angles  $\alpha_2$  and  $\alpha_4$  were found in a similar manner except the axial position of collimator 1b was utilized.
- 3) Figure (4.16) is a plot of ray traces from particles of selected energy emitted at  $\alpha_1$ ,  $\alpha_2$ ,  $\alpha_3$ , and  $\alpha_4$  for 1% transmission. Observe at  $r_{\text{rf}}$  that the beam width at collimator set 2 is described by traces of particles emitted from source positions ( $\pm r_{\text{disk}}, 0, -0.381$ ) at corresponding emission angles  $\alpha_2$  and  $\alpha_4$  respectively. In particular, the axial position of collimator 2a is found by performing a linear interpolation on the  $r$  versus  $z$  data about  $r_{\text{rf}}$  for a particle of selected energy emitted from ( $r_{\text{disk}}, 0, -0.381$ ) at angle  $\alpha_2$ . The axial position of collimator 2b is found in a similar manner except angle  $\alpha_4$  and source point ( $-r_{\text{disk}}, 0, -0.381$ ) are used. (NOTE: the preceding method of determining the axial positions of collimators 2a and 2b makes the maximum

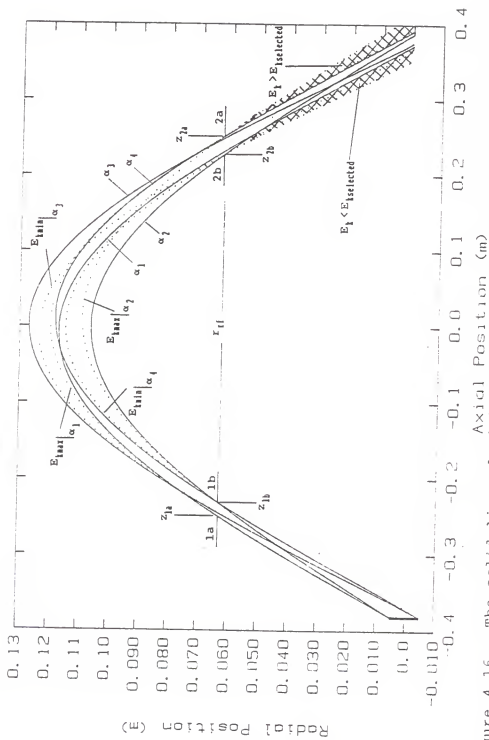


Figure 4.16. The solid lines depict ray traces of particles of selected energy (1 MeV) emitted at the extremum angles about the periphery of a disk source of diameter=1 cm. The dotted lines depict traces made by the maximum and minimum energy particles that contribute to the beam emitted from the extremum angles. The cross hatched region depicts portions of the beam that do not contain any particles of selected energy. Collimator sets 1 and 2 are configured for  $T=1\%$ .

utilization of all particles of selected energy emitted by a disk source for a specified transmission. Later a procedure for improving the resolution by narrowing the slit width between collimators 2a and 2b will be provided).

- 4) Finally the maximum and minimum contributing particle energies can be determined. To find  $E_{kmax}$ : particles of energies greater and less than the actual value of  $E_{kmax}$  were emitted from the source point  $(r_{disk,0}, -0.381)$  at angle  $\alpha_2$ . They were tracked to the axial position of collimator 2a where their radial positions were recorded. A linear interpolation was performed about the radial value  $r_{rf}$  yielding  $E_{kmax}$ . Similarly to find  $E_{kmin}$ : particles of energies greater and less than the actual value of  $E_{kmin}$  were emitted from the source point  $(-rdisk,0,-0.381)$  at angle  $\alpha_4$ . They were tracked to the axial position of collimator 2b where their radial positions were recorded. A linear interpolation was performed about the radial value  $r_{rf}$  yielding  $E_{kmin}$ . The dotted ray traces shown in fig. (4.16) represent particles of the maximum and minimum energy emitted at the specified extremum angle.

Tables (4.2a) and (4.2b) provide a summary of extremum angles, required positions of collimators 2a and 2b for maximum utilization of available selected energy particles, maximum and minimum particle energies contributing to the beam, and base-width resolution for a point source and disk sources of 0.1, 0.6, and 1.0 cm diameter. The data in each table are for a selected beam energy of 1 MeV: table (4.2a) is for 1% transmission while table (4.2b) is for 0.5% transmission. Figure (4.17) is based upon data compiled in tables (4.2a) and (4.2b) and depicts the base-width variation with source diameter and transmission. NOTE: the analysis for the case of a point source was different than for disk sources. The beam

Table 4.2a. The extremum angles, maximum and minimum particle energies contributing to the beam, and the theoretical base-width resolution for a point source and sources of diameter 0.1, 0.6, and 1.0 cm. All data are for a selected beam energy of 1 MeV and 1% transmission.

Source Diameter (cm)	Extremum Angles (degrees)				Axial Position of Collimator Set #2 (m)		$E_{\text{min}} \alpha_j$ (MeV)	$E_{\text{min}} \alpha_i$ (MeV)	Base-Width Resolution $R_B$ (%)
	$\alpha_1$	$\alpha_j$	$\alpha_j$	$\alpha_i$	2a	2b			
1.0	24.6	22.2	27.2 <sup>†</sup>	25.2	0.2509	0.2264	1.0415	0.9578	8.37
0.6	25.3	22.8	27.2 <sup>†</sup>	24.6	0.2470	0.2324	1.0253	0.9748	5.05
0.1	26.1	23.5	26.5	23.8	0.2413	0.2389	1.0042	0.9958	0.84
point source			$\alpha_{\text{min}} = \alpha + \Delta\alpha = 26.356$		0.2410	0.2401	1.0015	0.9985	0.30
			$\alpha_{\text{max}} = \alpha - \Delta\alpha = 23.644$						

<sup>†</sup> The acceptance angle of collimator 1a for selected energy particles is actually slightly larger. The  $\alpha_j$  angle values were decreased to the tabulated values because particles of selected energy would strike the vacuum chamber wall at the slightly larger actual angle.

Table 4.2b. The extremum angles, maximum and minimum particle energies contributing to the beam, and the theoretical base-width resolution for a point source and sources of diameter 0.1, 0.6, and 1.0 cm. All data are for a selected beam energy of 1 Mev and 0.5% transmission.

Source Diameter (cm)	Extremum Angles (degrees)				Axial Position of Collimator Set #2 (m)		$E_{\text{min}} \alpha_j$ (MeV)	$E_{\text{min}} \alpha_i$ (MeV)	Base-Width Resolution $R_b$ (%)
	$\alpha_1$	$\alpha_j$	$\alpha_j$	$\alpha_i$	2a	2b			
1.0	24.0	22.8	27.2 <sup>1</sup>	25.9	0.2505	0.2275	1.0382	0.9601	7.81
0.6	24.6	23.4	26.6	25.3	0.2469	0.2336	1.0229	0.9770	4.59
0.1	25.5	24.2	25.8	24.5	0.2419	0.2397	1.0039	0.9963	0.76
point source			$\alpha_{\text{min}} = \alpha_j = \Delta x = 25.678$		0.2410	0.2407	1.0004	0.9995	0.09
			$\alpha_{\text{max}} = \alpha_i = \Delta x = 24.322$						

<sup>1</sup> The acceptance angle of collimator 1a for selected energy particles is actually slightly larger. The  $\alpha_j$  angle values were decreased to the tabulated values because particles of selected energy would strike the vacuum chamber wall at the slightly larger actual angle.



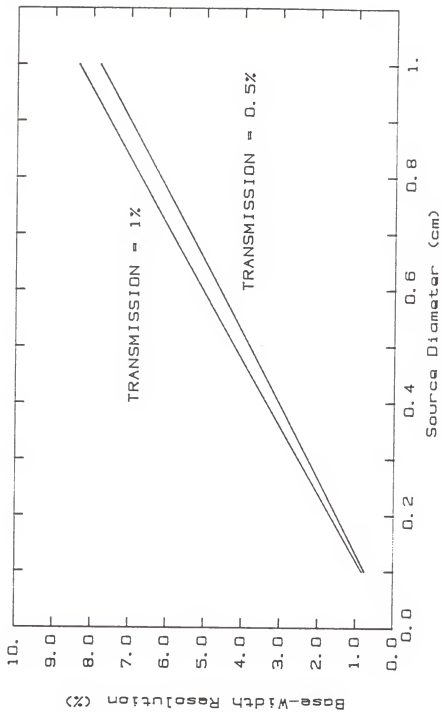


Figure 4.17. Theoretical base-width resolution as a function of disk source diameter for 0.5% and 1% transmission. Data are for the system configured with collimators 2a and 2b positioned to accept all particles of selected energy reaching collimator set 2.

width at the ring focus position is defined by ray traces of particles of selected energy emitted at angles  $\alpha$  and  $\alpha - \Delta\alpha$ , refer to fig. (4.9). The axial position of collimator 2a was based on tracking a particle of selected energy emitted at angle  $\alpha$ , while collimator 2b was based on tracking a particle of selected energy emitted at angle  $\alpha - \Delta\alpha$ . The maximum particle energy was determined for a particle emitted at angle  $\alpha - \Delta\alpha$  while the minimum energy was found for a particle emitted at the central-ray emission angle  $\alpha$ .

#### 4.4.1. RESOLUTION VARIATION WITH SELECTED BEAM ENERGY

As stated previously the base-width resolution is a strong function of selected beam energy. Figure (4.18) depicts the base-width resolution as a function of beam energy for 1% transmission and disk sources of diameter 0.1, 0.6, and 1.0 cm. The data for the figure was obtained by examining the trajectories of selected particle energies other than 1 MeV in the same manner as described previously.

#### 4.4.2 TECHNIQUE TO IMPROVE THE BASE WIDTH RESOLUTION

Improving the base-width resolution may be achieved by simply decreasing the slit width between collimators 2a and 2b regardless of the selected transmission. The following procedure may be followed to yield a desired base-width resolution about a selected energy:

- 1) Find extremum angles  $\alpha_2$  and  $\alpha_4$  for specified transmission and source diameter.
- 3) Find  $E_{kmax}$  and  $E_{kmin}$  for the desired base-width resolution using the equations

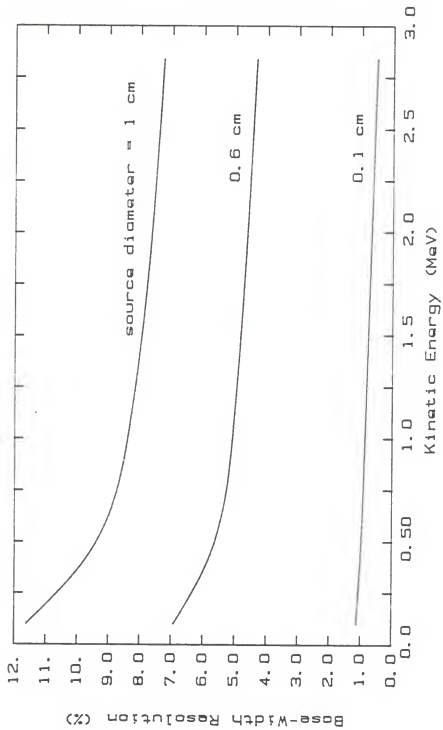


Figure 4.18. Theoretical base-width resolution as a function of source diameter and selected beam energy. Data are for the system configured for 1% transmission and with collimators 2a and 2b positioned to accept all particles of selected energy reaching collimator set 2.

$$E_{k\max} = E_{k\text{selected}} (1+R_b /2)$$

$$E_{k\min} = E_{k\text{selected}} (1-R_b /2).$$

- 4) Determine the required axial position of collimator 2a by making a r versus z ray trace of the maximum energy particle emitted at the source point  $(r_{\text{disk}},0,-0.381)$  at angle  $\alpha_2$ . Perform a linear interpolation of the r versus z data about the radial position  $r_{\text{rf}}=0.0628$  m to find the axial position of collimator 2a. Determine the required axial position of collimator 2b by making a r versus z ray trace of the minimum energy particle emitted at the source point  $(-r_{\text{disk}},0,-0.381)$  at angle  $\alpha_4$ . Perform a linear interpolation of the r versus z data about the radial position  $r_{\text{rf}}$  to find the axial position of collimator 2b.

It should be pointed out that if the slit width is decreased too much the resolution may decrease or else will remain constant while beam intensity decreases. This undesirable effect is the result of the increasing ratio of scattered particles from the collimator surfaces and structural components to uncollided particles in the beam as the slit width is decreased.

#### 4.4.3 OBSERVATIONS AND CONCLUSIONS REGARDING RESOLUTION

- 1) From tables (4.2a) and (4.2b) or fig. (4.17) observe that decreasing the transmission from 1% to 0.5% only yields an improvement in resolution of less than 10%. At the same time the beam intensity is decreased by approximately 50%; for this reason 1% transmission is a logical choice for configuring the collimators.
- 2) From fig. (4.17) the base-width resolution was shown to be a strong function of the disk source diameter.

- 3) From fig. (4.18) the base-width resolution was shown to be a strong function of selected beam energy.
- 4) A technique was provided for attaining a specified base-width resolution exceeding the values tabulated in tables (4.2a) and (4.2b).
- 5) The cross hatched portion of the beam shown in fig. (4.16) contains no particles of desired selected energy. Particles of energy greater and less than the selected energy, which are emitted from the periphery of a disk source, at emission angles ranging between the extremum angles are observed to form into distinct bands at the fringe of the beam. The base-width resolution can be improved without affecting the transmission of particles of selected energy by stripping the undesirable beam components by the use of additional exit window collimators. The previously quoted base-width resolutions are theoretically decreased by approximately a factor of 2 when the undesirable particles are stripped from the fringes of the beam.
- 6) The base-width resolutions quoted are indicative of the beam just after it passes through collimators 2a and 2b. Scattering from the collimators, MLMES structure, exit window aperture or mylar window, and air molecule scattering inside the vacuum chamber or between the detector and exit window are not accounted for. All of these unaccounted effects will add uncertainty to the theoretically quoted base-width resolution. Figure (4.19) depicts the peak broadening and energy shifting that occurs as a monoenergetic beam passes through air layers of different thicknesses.
- 7) Experimental results weren't available for KSU-MLMES#1 at the time of this thesis because the system was in the final construction phase. Figure (4.20) depicts nearly monoenergetic peaks generated by the Lawrence National

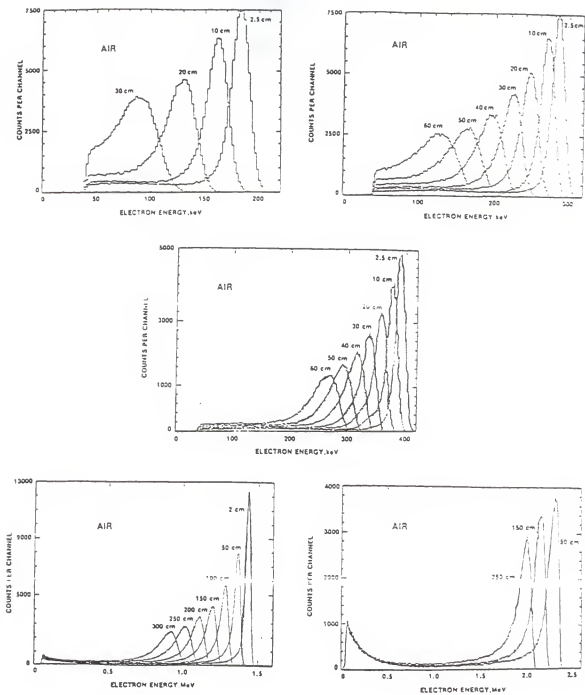


Figure 4.19. Monoenergetic electron peaks generated by the National Bureau of Standards 4 MeV Van de Graaff accelerator. Degradation in air of nominal 200 keV to 2.5 MeV electrons in different thicknesses of intervening air layers (16).

Electron energy spectra measured 4 cm from electron spectrometer's exit port.  
Magnet current: a) 1.75 amps, b) 2.50 amps, c) 3.00 amps, d) 4.05 amps

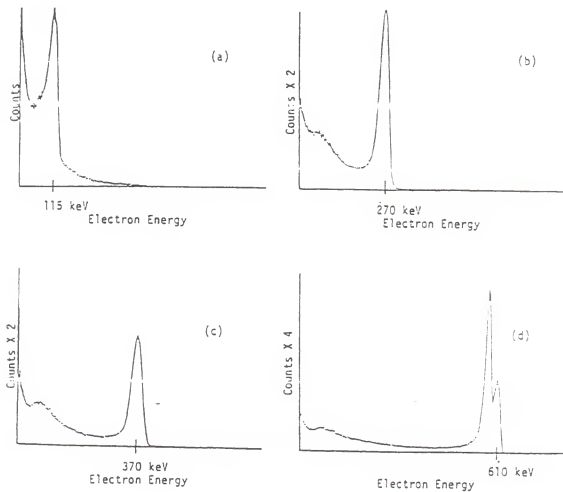


Figure 4.20. Monoenergetic electron peaks generated by the Lawrence National Laboratory magnetic lens monoenergetic electron source [9].

Laboratory monoenergetic electron source. The results were generated with their system configured with a 1.0 cm diameter, 20 mCi  $^{137}\text{Cs}$  source. Transmission and central-ray initial emission angle data weren't provided in their article. Based on their quoted exit beam diameter of 5.0 cm at a distance of 10.0 cm from the exit window, one can decipher that  $\alpha \approx 14^\circ$  for their system. The monoenergetic beam passed through a 3 mg/cm<sup>2</sup> thick mylar exit window, 4.0 cm of air, and a 10.0 mg/cm<sup>2</sup> Be detector entrance window before being recorded by an intrinsic Ge detector. Recall the work performed by Lindgren presented earlier in fig. (3.1) and the theoretical base-width resolution predictions summarized in tables (4.2a) and (4.2b). The evidence suggests that KSU-MLMES#1 will have the capability to exceed the performance of the LNL-MLMES.



## V. DETERMINATION OF THE POWER-SUPPLY STABILITY REQUIREMENTS

Any fluctuation in the electrical current about the selected focusing current will lead to a broadening of the peak width. To limit the peak base-width broadening to 0.1% the following analysis was performed in order to obtain the power-supply stability requirements. The derivative with respect to electric current of the spectrometer operating equation yields

$$\frac{\partial E_k}{\partial I} = \frac{kE_o I}{\sqrt{kI^2 + 1}} . \quad (5.1)$$

A plot of eq. (5.1) is provided in fig. (5.1). Next the allowed deviation in  $E_k$  for 0.1% broadening is determined. At a selected beam energy  $E_k=2.83686$  MeV, corresponding to a maximum focusing current of 50 A

$$dE_k = .5(.001) 2.83686 = 0.001418 \text{ MeV}.$$

The factor of .5 appearing in the expression arises to account for the  $\pm dI$  variation about the focusing current. Solving for  $dI$  from eq. (5.1) yields

$$|dI| = \frac{dE_k}{\left[ \frac{\partial E_k}{\partial I} \right]_{I=50A}} = \frac{0.001418}{0.06544} = 0.02167A .$$

Therefore the power-supply stability requirement for a focusing current of 50 A is

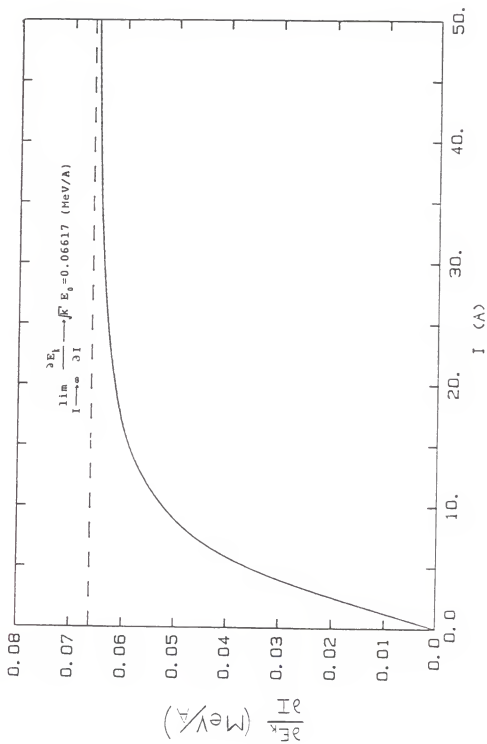


Figure 5.1. Selected beam energy dispersion as a function of electric current.

$(0.02167/50) \times 100\% = \pm 0.043\%$ . Similarly for a focusing current of 5 A the stability requirement is found to be  $\pm 0.027\%$ . The percentage stability requirements apply to any current fluctuation of duration greater than or equal to the particle transit time (defined as the elapsed time of a particle traveling along the central-ray trajectory between the source and focal point). At a focusing current of 50 A, the transit time of the corresponding 2.83686 MeV focused particle is approximately 2.845 ns while at 5 A and 0.09776 MeV focused particle the transit time is approximately 5.174 ns.

In summary: the power-supply stability requirement is observed to decrease as the focusing current increases. To limit peak broadening due to power-supply fluctuations to 0.1%, a power-supply of stability  $\pm 0.043\%$  at 50 A and  $\pm 0.027\%$  at 5 A should be used.

The actual power-supply stability requirements may be less restrictive. Recall in the previous analysis that the stability requirements were based upon the stringent base-width broadening limitation. Further, the inductive nature of the load (coil), will aid in power-supply stabilization.

## CONCLUSION

The theoretical design of a magnetic lens monoenergetic electron source was presented in this thesis. The work of Lindgren [11-13], regarding the relationship between magnetic field shape, resolution, and initial emission angle was examined. Based upon Lindgren's work and economic considerations, a MLMES with the source and focal points located near the ends of a coil and with a central-ray initial emission angle of  $25^{\circ}$  was selected.

A design procedure based upon the desired range of beam energies, minimum allowable magnetic focusing field, and uniform field trajectory equations was developed to estimate the required vacuum chamber dimensions. Next the dimensions and number of turns in the magnet coil were specified. Because the magnetic field shape utilized by the system was nonuniform, the operational characteristics of the system could only be determined numerically. A program titled PATH-RK4 was written to evaluate the trajectory of a beta-particle traveling through the nonuniform magnetic field.

Trajectory results from the program PATH-RK4 were used to find the source and focal point locations, ring focus point position, spectrometer operating equation, the angle at which the collimators must be beveled, and the resolution and transmission characteristics of the system. The base-width resolution of the system was investigated as a function of disk source diameter, transmission, and selected beam energy. As anticipated, the base-width resolution increased with source diameter, transmission, and decreasing selected beam energy.

## REFERENCES

1. P. Kapitza, Proc. Cambr. Phil. Soc., 22, 3, (1925).
2. R. Tricker, Proc. Cambr. Phil. Soc., 22, 454, (1925).
3. Clifford M. Witcher, Physics Review 60, 32, (1941).
4. O. Klemperer, Phil. Mag. 20, 259, (1940).
5. M. Deutsch, L.G. Elliot, and R.D. Evans, Rev. of Sci. Inst. 15, 178. (1944).
6. J.W.M. DuMond, Rev. of Sci. Inst., 20, 3, March (1949).
7. E. Persico, Rev. of Sci. Inst., 20, 3, March (1949).
8. F.H. Schmidt, Rev. of Sci. Inst., 23, 7, July (1952).
9. C.L. Graham and J.H. Elliot, "A Source of Monoenergetic Electrons for Beta Dosimetry", Proceedings of the International Beta Dosimetry Symposium, Washington D.C. (1983), U.S. Nuclear Regulatory Commission (NUREG/CP-0050), Jan (1984).
10. J. Mantel, "The Beta Ray Spectrum and the Average Beta Energy of Several Isotopes of Interest in Medicine and Biology", Int. J. App. Rad. and Isotopes. 23, 407-413.
11. I. Lindgren and W. Schneider, Nucl. Instr. Meth. 22, 48, (1963).
12. I. Lindgren, G. Patterson and W. Schneider, Nucl. Instr. Meth. 22, 61. (1963).
13. I. Lindgren, B. Olsen, G. Patterson and W. Schneider, Nucl. Instr. Meth. 41, 331. (1966).
14. Martin A. Plonus, Applied Electromagnetics, McGraw-Hill (1978).
15. Handbook of Mathematical, Scientific, and Engineering formulas, tables, functions, graphs, transforms, p. 897, Research and Education Association (1986).
16. "Standard Beta-Particle and Monoenergetic Electron Sources for the Calibration of Beta-Radiation Protection Instrumentation", U.S. Nuclear Regulatory Commission NUREG/CR-4266 and U.S. Dept. of Commerce/National Bureau of Standards NBSIR 85-3169 (1985).

APPENDIX A  
COMPUTER PROGRAMS

```

*****
* THE FOLLOWING FORTRAN PROGRAM NAMED "PATH-RK4" CALCULATES THE *
* TRAJECTORY OF A BETA PARTICLE TRAVELING THROUGH THE NONUNI- *
* FORM MAGNETIC FIELD OF THE MAGNETIC LENS MONOENERGETIC *
* ELECTRON SOURCE AT KANSAS STATE UNIVERSITY, DEPARTMENT OF *
* NUCLEAR ENGINEERING. THE PROGRAM MAY BE USED TO DESIGN NEW *
* OR ANALYZE ANY EXISTING MAGNETIC LENS SPECTROMETER SYSTEM *
* PROVIDED THE MAGNET COIL IS CONSTRUCTED OF A SINGLE COIL *
* WITH A RECTANGULAR SIDE-VIEW CROSS SECTION. *
* ALGORITHM: *
* THIS PROGRAM CALCULATES THE TRAJECTORY BY USING THE *
* RUNGE-KUTTA 4TH ORDER NUMERICAL METHOD TO SOLVE THE *
* NONLINEAR COUPLED EQUATIONS OF MOTION. *
* NOTE: THE PROGRAM WAS COMPILED USING THE MICROSOFT (R) *
* FORTRAN OPTIMIZING COMPILER VERSION 4.10. *
* AUTHOR: RICHARD WEINER *
* DATE: DECEMBER 31,1988 *
*****

```

```

      IMPLICIT REAL*8 (A-H,O-Z)
      CHARACTER QUEST1,QUEST2
      DIMENSION Y(6,4),F(6,4),W(16),ZER(16)

```

```

***** VARIABLE NOMENCLATURE *****
* PI=3.141592654 *
* U=PERMEABILITY OF FREE SPACE *
* Q=ELECTRONIC CHARGE (C) *
* C=SPEED OF LIGHT IN VACUUM (M/S) *
* RME=REST MASS OF ELECTRON (KG) *
* EM=ELECTRON MOVING MASS (KG) *
* CF=CONVERSION FACTOR (J/MEV) *
* V=VELOCITY MAGNITUDE (M/S) *
* EK=KINETIC ENERGY OF BETA PARTICLE (MEV) *
* SIZE=DISTANCE COVERED IN ONE TIME STEP (.01 M) *
* DELT=TIME STEP FOR THE TRAJECTORY CALCULATION (S) *
* CUR=ELECTRIC CURRENT THROUGH THE COIL (A) *
* ALPHA=INITIAL EMISSION ANGLE OF BETA PARTICLE (RADIAN) *
* N=NUMBER OF TURNS IN COIL (1196) *
* D=COIL LENGTH (M) *
* R1=INNER COIL RADIUS (M) ---LOWER INTEGRATION LIMIT ON R *
* R2=OUTER COIL RADIUS (M) ---UPPER INTEGRATION LIMIT ON R *
* PHI1=0 (RADIAN) ---LOWER INTEGRATION LIMIT ON PHI *
* PHI2=2*PI (RADIAN) ---UPPER INTEGRATION LIMIT ON PHI *
* FL=1/2 FOCAL LENGTH (M), DEFINED AS SOURCE TO Z=0 DISTANCE *
* RVAC=INSIDE RADIUS OF VACUUM CHAMBER *
*****

```

```

***** PROMPT USER FOR DATA *****

```

```

      WRITE(*,1)
1  FORMAT(1X,'DO YOU WANT TO USE DEFAULT COIL AND VACUUM'
& ' CHAMBER DIMENSIONS?',/,/,
& ' ENTER [Y/N] AND PRESS RETURN',/,/,
& ' DEFAULT COIL DIMENSIONS:LENGTH=.8509 M',/,/,

```

```

& ' INNER RADIUS=.1397 M,'//,
& ' OUTER RADIUS=.16345 M'//,
& ' # TURNS=1196'//,
& ' DEFAULT VACUUM CHAMBER DIMENSIONS:INNER RADIUS=.127 M,'
& ' LENGTH=1.016 M')
READ(*,'(A1)') QUEST1
IF (QUEST1 .EQ. 'N') THEN
WRITE(*,2)
2 FORMAT(1X,'ENTER COIL LENGTH (M)')
READ(*,'(F8.0)') D
WRITE(*,3)
3 FORMAT(1X,'ENTER COIL INNER RADIUS (M)')
READ(*,'(F8.0)') R1
WRITE(*,4)
4 FORMAT(1X,'ENTER COIL OUTER RADIUS (M)')
READ(*,'(F8.0)') R2
WRITE(*,5)
5 FORMAT(1X,'ENTER THE NUMBER OF TURNS IN THE COIL')
READ(*,'(I5)') N
WRITE(*,6)
6 FORMAT(1X,'ENTER THE VACUUM CHAMBER INNER RADIUS AND'
& ' LENGTH (M)')
READ(*,'(2F8.0)') RVAC,ZVAC
ELSE
* DEFAULT COIL DIMENSIONS
D=.8509
R1=.1397
R2=.16345
N=1196
* DEFAULT VACUUM CHAMBER DIMENSIONS
RVAC=.127
ZVAC=1.016
END IF

WRITE(*,7)
7 FORMAT(/,1X,'DO YOU WANT TO USE DEFAULT PARTICLE INITIAL'
& ' POSITION?',//,
& ' ENTER [Y/N] AND PRESS RETURN',//,
& ' DEFAULT POSITION:X(0)=0 M,'//,
& ' Y(0)=0 M,'//,
& ' Z(0)=-.381 M')
READ(*,'(A1)') QUEST2
IF (QUEST2 .EQ. 'N') THEN
WRITE(*,8)
8 FORMAT(1X,'ENTER THE INITIAL POSITION: X(0),Y(0),Z(0)')
READ(*,'(3F8.0)') XINIT,YINIT,ZINIT
RINIT=(XINIT**2+YINIT**2)**.5
ELSE
* DEFAULT INITIAL POSITION
XINIT=0
YINIT=0
ZINIT=-.381
RINIT=0

```



```

END IF

WRITE(*,9)
9 FORMAT(/,1X,'ENTER PARTICLE KINETIC ENERGY (MEV)')
READ (*,'(F8.0)') EK
WRITE(*,10)
10 FORMAT(1X,'ENTER ELECTRIC CURRENT (AMPS)')
READ (*,'(F8.0)') CUR
WRITE(*,11)
11 FORMAT(1X,'ENTER INITIAL EMISSION ANGLE (DEGREES)')
READ (*,'(F8.0)') ANGLE

WRITE(*,12)
12 FORMAT(/,1X,'SELECT TRAJECTORY CONVERGENCE CRITERION'
& ' OPTION 1 OR 2',/,
& '      1) TRACK PARTICLE TO FOCAL POINT (I.E. STOP',/,
& '      TRACKING PARTICLE ONCE IT REACHES A MINIMUM',/,
& '      RADIAL VALUE ALONG THE TRAJECTORY)',/,
& '      2) TRACK PARTICLE TO A USER DEFINED FINAL AXIAL',/,
& '      POSITION',/)
READ (*,'(I1)') IFLAG

IF (IFLAG .EQ. 2) THEN
WRITE(*,13)
13 FORMAT(/,1X,'ENTER THE FINAL AXIAL POSITION TO WHICH',/,
& ' THE PARTICLE IS TO BE TRACKED (METERS)')
READ (*,'(F8.0)') ZFINAL
END IF

***** OPEN DISK FILES FOR DATA OUTPUT *****

OPEN(UNIT=1, FILE='A:XZ')
OPEN(UNIT=2, FILE='A:YZ')
OPEN(UNIT=3, FILE='A:XY')
OPEN(UNIT=4, FILE='A:RZ')
OPEN(UNIT=5, FILE='A:VXZ')
OPEN(UNIT=6, FILE='A:VYZ')
OPEN(UNIT=7, FILE='A:VZZ')
OPEN(UNIT=8, FILE='A:BRZ')
OPEN(UNIT=9, FILE='A:BZZ')
OPEN(UNIT=10, FILE='A:XYZ')

* CONVERT INITIAL EMISSION ANGLE FROM DEGREES TO RADIANS
PI=2*ASIN(1.)
ALPHA=ANGLE*PI/180.

FL=ABS(ZINIT)
U=4*PI*1E-07
Q=-1.6021892E-19
C=2.99792458E8
RME=9.109534E-31
CF=1.6021892E-13
EM=EK*CF/C**2+RME

```

```

QDM=Q/EM
V=C*(1-(RME/EM)**2)**.5
SIZE=.01
DELT=SIZE/V
UNI=U*N*CUR
PHI1=0
PHI2=2*PI
CONST=(UNI/(4*PI*D*(R2-R1)))*.25*(PHI2-PHI1)*(R2-R1)

```

\*\*\*\*\* GAUSS-QUADRATURE WEIGHTS AND ZEROS \*\*\*\*\*

```

DATA(ZER(I),I=1,8)/ .095012509837637, .281603550779259,
& .458016777657227, .617876244402644, .755404408355003,
& .865631202387832, .944575023073233, .989400934991649/
DATA(W(I),I=1,8)/ .189450610455068, .182603415044924,
& .169156519395003, .149595988816577, .124628971255534,
& .095158511682494, .062253523938648, .027152459411754/
DO 100 I=1,8
ZER(I+8)=-ZER(I)
100 W(I+8)=W(I)

```

\*\*\*\*\*

\* THE PROGRAM UTILIZES THE CURRENT AND PREVIOUS THREE VALUES OF  
\* THE PARTICLE'S POSITION IN CYLINDRICAL COORDINATES IN ORDER  
\* THAT A DETERMINATION CAN BE MADE REGARDING TRAJECTORY CONVER-  
\* GENCE TO THE FOCAL POINT: INITIALIZE THE VALUES OF THESE POINTS.

```

RNEW=0
ROLD1=0
ROLD2=0
ROLD3=0
ZNEW=-FL
ZOLD1=0
ZOLD2=0
ZOLD3=0

```

\*\*\*\*\*

\* THE PROGRAM UTILIZES THE PREVIOUS THREE VALUES OF THE PARTI-  
\* CLE'S VELOCITY COMPONENTS IN RECTANGULAR COORDINATES IN ORDER  
\* THAT THEY MAY BE EVALUATED AT THE FOCAL POINT: INITIALIZE THE  
\* VALUES OF THESE POINTS.

```

VXNEW=V*SIN(ALPHA)
VXOLD1=0
VXOLD2=0
VXOLD3=0
VYNEW=0
VYOLD1=0
VYOLD2=0
VYOLD3=0
VZNEW=V*COS(ALPHA)
VZOLD1=0
VZOLD2=0
VZOLD3=0

```

```

***** RUNGE-KUTTA 4TH ORDER METHOD *****
* THE RUNGE-KUTTA 4TH ORDER METHOD IS USED TO SOLVE THE 6 *
* COUPLED NONLINEAR EQUATIONS OF MOTION IN RECTANGULAR COORD- *
* INATES. THE FOLLOWING NOTATION IS USED: *
* Y(1,J)=VX F(1,J)=(Q/M)*(VY*BZ-VZ*BY) *
* Y(2,J)=VY F(2,J)=(Q/M)*(VZ*BX-VX*BZ) *
* Y(3,J)=VZ F(3,J)=(Q/M)*(VX*BY-VY*BX) *
* Y(4,J)=X F(4,J)=VX *
* Y(5,J)=Y F(5,J)=VY *
* Y(6,J)=Z F(6,J)=VZ *
*****

```

```

***** INITIAL CONDITIONS *****

```

```

Y(1,1)=V*SIN(ALPHA)
Y(2,1)=0
Y(3,1)=V*COS(ALPHA)
Y(4,1)=XINIT
Y(5,1)=YINIT
Y(6,1)=ZINIT
P=RINIT

```

```

WRITE(1,1020) Y(6,1),Y(4,1)
WRITE(2,1020) Y(6,1),Y(5,1)
WRITE(3,1020) Y(5,1),Y(4,1)
WRITE(4,1020) Y(6,1),P
WRITE(5,1010) Y(6,1),Y(1,1)
WRITE(6,1010) Y(6,1),Y(2,1)
WRITE(7,1010) Y(6,1),Y(3,1)
WRITE(10,1030) Y(4,1),Y(5,1),Y(6,1)
1010 FORMAT(1X,F9.6,1X,E16.9)
1030 FORMAT(1X,F9.6,1X,F9.6,1X,F9.6)

```

```

* TIME STEP LOOP

```

```

DO 15 LOOP=1,1000

```

```

* RK4 HORNER EVALUATION LOOP

```

```

DO 20 J=1,4

```

```

***** MAGNETIC FIELD EVALUATION *****
* THIS PORTION OF THE PROGRAM UTILIZES 16-POINT GAUSS-QUADRATURE*
* DOUBLE NUMERICAL INTEGRATION TO CALCULATE THE RADIAL AND AXIAL*
* COMPONENTS OF THE MAGNETIC FIELD AT THE SPECIFIED PARTICLE *
* POSITION. *
*****

```

```

P=(Y(4,J)**2+Y(5,J)**2)**.5
H=Y(6,J)
SUM2A=0
SUM2B=0
DO 200 N=1,16

```

```

R=.5*(R2+R1+(R2-R1)*ZER(N))
SUM1A=0
SUM1B=0
DO 210 K=1,16
PHI=.5*(PHI2+PHI1+(PHI2-PHI1)*ZER(K))
V1=R*COS(PHI)
V2=R**2+P**2-2*P*V1
V3=(V2+(H-D/2.）**2)**(-.5)
V4=(V2+(H+D/2.）**2)**(-.5)
SUM1A=SUM1A+W(K)*V1*(V3-V4)
SUM1B=SUM1B+W(K)*((P*V1-R**2)/V2)*((H-D/2.)*V3-(H+D/2.)*V4)

210 CONTINUE
SUM2A=SUM2A+W(N)*SUM1A
SUM2B=SUM2B+W(N)*SUM1B
200 CONTINUE
BR=CONST*SUM2A
BZ=CONST*SUM2B

IF (J .EQ. 1 .AND. FLAG .NE. 1) THEN
WRITE(8,1020) H,BR
WRITE(9,1020) H,BZ
1020 FORMAT(1X,E16.9,1X,E16.9)
END IF

```

\* EXPRESS RADIAL COMPONENT OF MAGNETIC FIELD IN RECTANGULAR  
\* COORDINATES

```

IF (P .EQ. 0) THEN
BX=0
BY=0
ELSE
BX=BR*Y(4,J)/P
BY=BR*Y(5,J)/P
END IF

```

\*\*\*\*\*

```

F(1,J)=QDM*(Y(2,J)*BZ-Y(3,J)*BY)
F(2,J)=QDM*(Y(3,J)*BX-Y(1,J)*BZ)
F(3,J)=QDM*(Y(1,J)*BY-Y(2,J)*BX)
F(4,J)=Y(1,J)
F(5,J)=Y(2,J)
F(6,J)=Y(3,J)

```

```

IF (J .LT. 3) THEN
DO 30 I=1,6
30 Y(I,J+1)=Y(I,1)+DELT*F(I,J)/2.
ELSE IF (J .EQ. 3) THEN
DO 40 I=1,6
40 Y(I,J+1)=Y(I,1)+DELT*F(I,J)
ELSE
DO 50 I=1,6
50 Y(I,1)=Y(I,1)+DELT*(F(I,1)/2.+F(I,2)+F(I,3)+F(I,4)/2.)/3.
END IF
20 CONTINUE

```

\* KEEP TRACK OF PREVIOUS THREE PARTICLE POSITIONS

ZOLD3=ZOLD2  
ZOLD2=ZOLD1  
ZOLD1=ZNEW  
ROLD3=ROLD2  
ROLD2=ROLD1  
ROLD1=RNEW

\* KEEP TRACK OF PREVIOUS THREE PARTICLE VELOCITY COMPONENTS

VXOLD3=VXOLD2  
VXOLD2=VXOLD1  
VXOLD1=VXNEW  
VXNEW=Y(1,1)  
VYOLD3=VYOLD2  
VYOLD2=VYOLD1  
VYOLD1=VYNEW  
VYNEW=Y(2,1)  
VZOLD3=VZOLD2  
VZOLD2=VZOLD1  
VZOLD1=VZNEW  
VZNEW=Y(3,1)

\*\*\*\*\* TRAJECTORY CONVERGENCE TEST \*\*\*\*\*  
\* THE CONVERGENCE TEST IS BASED UPON FINDING THE LOCATION WHERE \*  
\* THE MINIMUM RADIAL COMPONENT OF THE HELICAL TRAJECTORY OCCURS \*  
\* AND CONSIDERING THIS LOCATION AS THE FOCAL POINT. \*  
\*\*\*\*\*

RNEW=(Y(4,1)\*\*2+Y(5,1)\*\*2)\*\*.5  
ZNEW=Y(6,1)

\* TEST FOR FLAG ALREADY SET: THIS INDICATES THAT THE LAST DATA  
\* POINT HAS BEEN ACQUIRED AND THE FOCAL POINT CAN BE EVALUATED

IF (FLAG .EQ. 1) THEN  
GOTO 70  
END IF

\* CHECK TO SEE IF PARTICLE HAS STRUCK THE VACUUM CHAMBER WALL

IF (RNEW .GE. RVAC .AND. ZNEW .LE. ZVAC/2.) THEN  
WRITE(\*,60) ZNEW  
60 FORMAT(1X,'THE PARTICLE HAS STRUCK THE WALL AT Z=',F9.6)  
GOTO 2000  
END IF

\*\*\*\*\* FOR THE CASE OF IFLAG=OPTION 2 \*\*\*\*\*

IF (IFLAG .EQ. 2) THEN  
\* CHECK FOR PARTICLE CONVERGENCE  
IF (ZNEW .GT. ZFINAL) THEN

```

RFINAL=RNEW-(RNEW-ROLD1)*(ZNEW-ZFINAL)/(ZNEW-ZOLD1)
VXFIN=VXNEW-(VXNEW-VXOLD1)*(ZNEW-ZFINAL)/(ZNEW-ZOLD1)
VYFIN=VYNEW-(VYNEW-VYOLD1)*(ZNEW-ZFINAL)/(ZNEW-ZOLD1)
VZFIN=VZNEW-(VZNEW-VZOLD1)*(ZNEW-ZFINAL)/(ZNEW-ZOLD1)
WRITE(4,1020) ZFINAL,RFINAL
WRITE(5,1010) ZFINAL,VXFIN
WRITE(6,1010) ZFINAL,VYFIN
WRITE(7,1010) ZFINAL,VZFIN
GOTO 2000
END IF
* PARTICLE HAS NOT CONVERGED
GOTO 80
END IF
*****
* WHEN PARTICLE NEARS THE FOCAL POINT DECREASE THE TIME STEP IN
* ORDER TO INCREASE ACCURACY OF FOCAL POINT COORDINATES
* EVALUATION
IF (RNEW .LT. .015 .AND. ZNEW. GT. .1) THEN
SIZE=.002
DELT=SIZE/V
END IF
IF (RNEW .GT. ROLD1 .AND. ZNEW .GT. .1) THEN
* PARTICLE HAS CONVERGED: CHECK TO SEE IF ONE MORE STEP REQUIRED
IF (RNEW .GT. ROLD2) THEN
* FINISHED: NO MORE STEPS REQUIRED
GOTO 70
ELSE
* NEED ONE MORE STEP: SET FLAG=1
FLAG=1
GOTO 15
END IF
ELSE
* PARTICLE HAS NOT CONVERGED
GOTO 80
END IF
70 SLOPE1=(ROLD2-ROLD3)/(ZOLD2-ZOLD3)
SLOPE2=(RNEW-ROLD1)/(ZNEW-ZOLD1)
B1=ROLD2-ZOLD2*SLOPE1
B2=RNEW-ZNEW*SLOPE2
* COORDINATES OF FOCAL POINT
ZFL=(B2-B1)/(SLOPE1-SLOPE2)
RFL=.5*((SLOPE1+SLOPE2)*ZFL+B1+B2)
WRITE(4,1020) ZFL,RFL
* VELOCITY COMPONENTS AT FOCAL POINT
DENOM=1/(ZFL-ZOLD3)-1/(ZFL-ZOLD2)
VXFL=(VXOLD3/(ZFL-ZOLD3)-VXOLD2/(ZFL-ZOLD2))/DENOM
VYFL=(VYOLD3/(ZFL-ZOLD3)-VYOLD2/(ZFL-ZOLD2))/DENOM

```

```

VZFL=(VZOLD3/(ZFL-ZOLD3)-VZOLD2/(ZFL-ZOLD2))/DENOM
WRITE(5,1010) ZFL,VXFL
WRITE(6,1010) ZFL,VYFL
WRITE(7,1010) ZFL,VZFL

* CALCULATE THE FOCAL LENGTH

FLEN=FL+ZFL
WRITE(*,1000) FLEN
1000 FORMAT(1X,'FOCAL LENGTH=',E16.9)
GOTO 2000

80 WRITE(1,1020) Y(6,1),Y(4,1)
WRITE(2,1020) Y(6,1),Y(5,1)
WRITE(3,1020) Y(5,1),Y(4,1)
WRITE(4,1020) ZNEW,RNEW
WRITE(5,1010) Y(6,1),Y(1,1)
WRITE(6,1010) Y(6,1),Y(2,1)
WRITE(7,1010) Y(6,1),Y(3,1)
WRITE(10,1030) Y(4,1),Y(5,1),Y(6,1)

* CONTINUE STEPPING FORWARD IN TIME UNTIL THE PARTICLE REACHES
* THE FOCAL POINT.
15 CONTINUE
2000 STOP
END

```

```

*****
* THE FOLLOWING FORTRAN PROGRAM NAMED "FIELD" CALCULATES THE
* MAGNETIC FIELD AT ANY LOCATION INSIDE THE MAGNETIC LENS MONO-
* ENERGETIC ELECTRON SOURCE AT KANSAS STATE UNIVERSITY. THE
* PROGRAM IS GENERAL IN NATURE AND MAY BE USED TO DETERMINE THE
* MAGNETIC FIELD INSIDE OF ANY SOLENOID WITH A RECTANGULARLY
* SHAPED CROSS SECTION.
* REQUIRED INPUTS:
* 1) POSITION IN CYLINDRICAL COORDINATES:(P,H)
* P CAN BE ANY VALUE
* H CAN BE ANY VALUE
* H=0 IS IN CENTER OF SOLENOID
* 2) ELECTIC CURRENT FLOWING THROUGH THE COIL:(CUR) (AMPERES)
* OUTPUT:
* 1) RADIAL MAGNETIC FIELD COMPONENT: BR (TESLAS)
* 2) AXIAL MAGNETIC FIELD COMPONENT: BZ (TESLAS)
* ALGORITHM:
* THE MAGNETIC FIELD EQUATIONS WERE DEVELOPED BY SOLVING
* THE THE BIOT-SAVART LAW IN CYLINDRICAL COORDINATES.
* THE FIELD COMPONENTS (BR AND BZ) EACH REQUIRED A TRIPLE
* INTEGRATION (I.E. OVER THE THREE CYLINDRICAL COORDINATES).
* THE INTEGRATION OVER THE Z DIRECTION WAS PERFORMED ANAL-
* YTICALLY WHILE THE INTEGRATION OVER THE R AND PHI
* DIRECTIONS IS PERFORMED NUMERICALLY BY GAUSS-QUADRATURE
* NOTE: THE PROGRAM WAS COMPILED WITH THE MICROSOFT (R) FORTRAN
* OPTIMIZING COMPILER VERSION 4.10.
* AUTHOR: RICHARD WEINER
* DATE: MARCH 19, 1988
*****

```

```

IMPLICIT REAL*8 (A-H,O-Z)
CHARACTER QUEST1
DIMENSION X(16),W(16)

```

```

***** VARIABLE NOMENCLATURE *****
* PI=3.141592654
* U=PERMEABILITY OF FREE SPACE
* CUR=ELECTRIC CURRENT THROUGH THE COIL (A)
* UNI=(PERMEABILITY)*(# TURNS IN COIL (1198))*(ELECTRIC CURRENT)
* D=COIL LENGTH (M)
* R1=INNER COIL RADIUS (M) ---LOWER INTEGRATION LIMIT ON R
* R2=OUTER COIL RADIUS (M) ---UPPER INTEGRATION LIMIT ON R
* PHI1=0 (RADIAN) ---LOWER INTEGRATION LIMIT ON PHI
* PHI2=2*PI (RADIAN) ---UPPER INTEGRATION LIMIT ON PHI
*****

```

```

***** PROMPT USER FOR DATA *****

```

```

WRITE(*,1)
1 FORMAT(1X,'DO YOU WANT TO USE DEFAULT COIL DIMENSIONS FOR THE'
& ' MLMES?',/,/,
& ' ENTER [Y/N] AND PRESS RETURN',/,/,
& ' DEFAULT COIL DIMENSIONS:LENGTH=.8509 M',/,/,
& ' INNER RADIUS=.1397 M',/,/,
)

```



```

& '                                OUTER RADIUS=.16345 M',/,/
& '                                # TURNS IN COIL=1196.',/,/)
  READ(*,'(A1)') QUEST1
  IF (QUEST1 .EQ. 'N') THEN
  WRITE(*,2)
2  FORMAT(1X,'ENTER COIL LENGTH (M)')
  READ(*,'(F8.0)') D
  WRITE(*,3)
3  FORMAT(1X,'ENTER COIL INNER RADIUS (M)')
  READ(*,'(F8.0)') R1
  WRITE(*,4)
4  FORMAT(1X,'ENTER COIL OUTER RADIUS (M)',/,/)
  READ(*,'(F8.0)') R2
  WRITE(*,5)
5  FORMAT(1X,'ENTER THE NUMBER OF TURNS IN COIL')
  READ(*,'(I5)') N
  ELSE
* DEFAULT COIL DIMENSIONS
  D=.8509
  R1=.1397
  R2=.16345
  N=1196
  END IF

  WRITE(*,6)
6  FORMAT(1X,'SELECT OPTION (1,2 OR 3)',/,/,
& '    1) EVALUATE RADIAL AND AXIAL FIELD COMPONENTS AT A',/,/
& '    SINGLE POINT',/,/
& '    2) EVALUATE RADIAL AND AXIAL FIELD COMPONENTS ALONG',/,/
& '    A LONGITUDINAL LINE (I.E. VARY AXIAL POSITION',/,/
& '    WHILE KEEPING RADIAL POSITION CONSTANT)',/,/
& '    3) EVALUATE RADIAL AND AXIAL FIELD COMPONENTS ALONG',/,/
& '    A TRANSVERSE LINE (I.E. VARY RADIAL POSITION WHILE',/,/
& '    KEEPING AXIAL POSITION CONSTANT)',/,/)
  READ(*,'(F8.0)') OPT1

  WRITE(*,7)
7  FORMAT(1X,'ENTER ELECTRIC CURRENT FLOWING THROUGH COIL (A)')
  READ(*,'(F8.0)') CUR

  IF (OPT1 .EQ. 1) THEN
  WRITE(*,8)
8  FORMAT(1X,'ENTER RADIAL AND AXIAL POSITION COORDINATES (P,H)')
& '  IN METERS',/,)
  READ(*,'(2F8.0)') P,H
  GOTO 15
  END IF

  IF (OPT1 .EQ. 2) THEN
  WRITE(*,9)
9  FORMAT(1X,'ENTER RADIAL POSITION VALUE IN METERS')
  READ(*,'(F8.0)') P
  WRITE(*,10)
10 FORMAT(1X,'ENTER INITIAL AND FINAL AXIAL POSITION VALUES'

```

```

& ' (INITIAL,FINAL) IN METERS',/)
  READ(*,'(2F8.0)') HMIN,HMAX
  GOTO 15
END IF

  IF (OPT1 .EQ. 3) THEN
    WRITE(*,11)
11  FORMAT(1X,'ENTER AXIAL POSITION VALUE IN METERS')
    READ(*,'(F8.0)') H
    WRITE(*,12)
12  FORMAT(1X,'ENTER INITIAL AND FINAL RADIAL POSITION VALUES',/,
& ' (INITIAL,FINAL) IN METERS: TYPICALLY (0,RMAX)',//)
    READ(*,'(2F8.0)') PMIN,PMAX
    END IF
15  CONTINUE

  PI=2*ASIN(1.)
  U=4*PI*1E-07
  UNI=U*1198*CUR
  PHI1=0
  PHI2=2*PI
  CONST=UNI/(4*PI*D*(R2-R1))

***** GAUSS QUADRATURE WEIGHTS AND ZEROS *****
  DATA(X(I),I=1,8)/ .095012509837637,.281603550779259,
& .458016777657227,.617876244402644,.755404408355003,
& .865631202387832,.944575023073233,.989400934991649/
  DATA(W(I),I=1,8)/ .189450610455068,.182603415044924,
& .169156519395003,.149595988816577,.124628971255534,
& .095158511682494,.062253523938648,.027152459411754/
  DO 50 J=1,8
  X(J+8)=-X(J)
50  W(J+8)=W(J)

***** OPEN DISK FILES FOR DATA OUTPUT *****

  IF (OPT1 .EQ. 1) GOTO 25
  OPEN(UNIT=1,FILE='A:BR')
  OPEN(UNIT=2,FILE='A:BZ')
25  CONTINUE
  IF (OPT1 .EQ. 1) GOTO 20
  DO 1000 MM=-100,100
  IF (OPT1 .EQ. 2) THEN
    H=(HMAX-HMIN)*MM/200.
  ELSE
    P=(PMAX-PMIN)*(100+MM)/200.
  END IF
20  CONTINUE

*****
* CALCULATE RADIAL AND AXIAL MAGNETIC FIELD COMPONENTS IN CYLINDRICAL
* COORDINATES:BR AND BZ
  V1=H-D/2.

```

```

V1A=V1**2
V2=H+D/2.
V2A=V2**2
SUM2A=0
SUM2B=0
DO 100 N=1,16
R=.5*(R2+R1+(R2-R1)*X(N))
SUM1A=0
SUM1B=0
DO 110 K=1,16
PHI=.5*(PHI2+PHI1+(PHI2-PHI1)*X(K))
V3=COS(PHI)
V4=R*V3
V5=R**2+P**2-2*P*V4
V6=V5+V1A
V6A=V6**(-.5)
V7=V5+V2A
V7A=V7**(-.5)
V8=R*(P*V3-R)
V9=V8/V5
SUM1A=SUM1A+W(K)*(V4*(V6A-V7A))
SUM1B=SUM1B+W(K)*(V9*(V1*V6A-V2*V7A))
110 CONTINUE
SUM2A=SUM2A+W(N)*SUM1A
SUM2B=SUM2B+W(N)*SUM1B
100 CONTINUE
CONST1=.25*(PHI2-PHI1)*(R2-R1)
BR=CONST*CONST1*SUM2A
BZ=CONST*CONST1*SUM2B
*****
* WRITE OUTPUT TO SCREEN OR DISK FILES
  IF (OPT1 .EQ. 1) THEN
    WRITE(*,30)BR,BZ
  30 FORMAT(1X,'BR=',E16.9,1X,'BZ=',E16.9)
  ELSE IF (OPT1 .EQ. 2) THEN
    WRITE(1,40) H,BR/CUR
    WRITE(2,40) H,BZ/CUR
  ELSE
    WRITE(1,40) P,BR/CUR
    WRITE(2,40) P,BZ/CUR
  END IF
  40 FORMAT(1X,E16.9,1X,E16.9)
  IF (OPT1 .EQ. 1) GOTO 2000
1000 CONTINUE
2000 STOP
      END

```

## APPENDIX B

### DERIVATION OF THE APPROXIMATE AVERAGE AXIAL MAGNETIC FIELD COMPONENT INSIDE A SOLENOIDAL COIL OF FINITE LENGTH

The axial component of the magnetic field along the axis of a solenoidal coil of effective radius  $a=(R_1+R_2)/2$ , may be derived from the expression for  $B_z(p,h)$  obtained in the section DERIVATION OF THE MAGNETIC FLUX-DENSITY VECTOR. Recall that we used the relation,  $\vec{Id}\vec{l}=\vec{J}d\vec{V}$ , where the magnitude of the current-density is  $J=NI/(D(R_2-R_1))$  and  $dV=rdrd\phi dz$  in the derivation of  $B_z(p,h)$ . For the simplified case of a coil of effective radius one obtains,  $\vec{Id}\vec{l}=\vec{J}d\vec{A}$ , where the magnitude of the current-density is  $J=NI/D$  and  $dA=r d\phi dz$ . Since we are assuming a coil of no thickness, we set  $r=\text{constant}$  effective radius ( $a$ ) wherever  $r$  appears in the expression for  $B_z(p,h)$ , and note that the integration over the radial direction is eliminated. Since we are only interested in the field along the axis of the solenoid, we set  $p=0$  in the expression for  $B_z(p,h)$ . These simplifications lead to the following analytic integral

$$B_z(0,h) = \frac{\mu_0 NI}{4\pi D} \int_{\phi=0}^{2\pi} \left[ \frac{(h+D/2)}{\sqrt{a^2+(h+D/2)^2}} - \frac{(h-D/2)}{\sqrt{a^2+(h-D/2)^2}} \right] d\phi.$$

Perform the integration and obtain

$$B_z(z) = \frac{\mu_0 NI}{2D} \left[ \frac{(z+D/2)}{\sqrt{a^2+(z+D/2)^2}} - \frac{(z-D/2)}{\sqrt{a^2+(z-D/2)^2}} \right],$$

where we have made a variable change from  $h$  to  $z$  in the result.

Now we are ready to determine an approximate average value of the axial component of the magnetic field inside a solenoid of finite length. The result we obtain is only an approximation because  $B_z(z)$  along the axis is assumed over the

entire volume within the solenoid, i.e. note that the variation of  $B_z$  with the radial direction has been neglected. The average value of the axial component of the field within a solenoid of finite length is given as

$$B_{z_{av}} = \frac{1}{D} \int_{z=-D/2}^{D/2} B_z(z) dz .$$

The integral may be solved analytically and the result is

$$B_{z_{av}} = \frac{\mu_0 NI}{D^2} \left[ \sqrt{a^2 + D^2} - a \right] .$$

DESIGN OF A MAGNETIC LENS  
MONOENERGETIC ELECTRON SOURCE

by

RICHARD A. WEINER

B.S. in N.E., Kansas State University, 1987

B.S. in E.E., Kansas State University, 1989

---

AN ABSTRACT OF A MASTER'S THESIS

submitted in partial fulfillment of the  
requirements for the degree

MASTER OF SCIENCE

Department of Nuclear Engineering

Kansas State University

Manhattan, Kansas

1989

## ABSTRACT

The theoretical design of a continuously selectable 100 keV to 2.8369 MeV monoenergetic electron source was developed based upon the concept of a magnetic lens spectrometer. The topics of selection of an appropriate magnetic field shape and central-ray initial emission angle were considered. The system designed utilized a nonuniform magnetic field, central-ray initial emission angle of  $25^\circ$ , and central-ray trajectory focal length of 0.762 m. A computer program named PATH-RK4 was developed to provide the precise trajectory of a beta-particle traveling through the nonuniform magnetic field generated by a single solenoidal coil of finite length. The code is general in nature and may be used to characterize the operational characteristics of any existing magnetic lens spectrometer or design new systems provided they consist of a single rectangularly shaped magnet coil of arbitrary dimensions.

A detailed examination of the resolution and transmission characteristics are provided for the proposed system. The base-width resolution and the required system collimator positions as a function of source diameter, transmission and selected beam energy were investigated.